Astron. Astrophys. 362, 169–188 (2000)

ASTRONOMY AND ASTROPHYSICS

Active eclipsing binary RT Andromedae revisited

T. Pribulla[1], **D. Chochol**[1], **L. Milano**[2,3], **L. Errico**[4], **A.A. Vittone**[4], **F. Barone**[2,3], **and Š. Parimucha**[1]

[1] Astronomical Institute of the Slovak Academy of Sciences, 059 60 Tatranská Lomnica, Slovakia (pribulla@ta3.sk)
[2] Dipartimento di Scienze Fisiche, Universita di Napoli "Federico II", Via Cinthia, 80126 Napoli, Italy
[3] Instituto Nazionale di Fisica Nucleare, Via Cinthia, 80126 Napoli, Italy
[4] Osservatorio Astronomico di Capodimonte, Via Moiariello 16, 80131 Napoli, Italy

Received 25 January 2000 / Accepted 11 August 2000

Abstract. All available photometric and spectroscopic data of the short-period RS CVn-like binary RT And have been reanalyzed in a homogeneous way. The long-term orbital period change is explained by two period jumps, a continuous period decrease combined with the light-time orbit or two light-time orbits. UBVRIJK light curves without maculation effects together with the radial velocities of both components were analysed with the Wilson-Devinney program to compute the photometric and spectroscopic elements and derive the masses of the components: m_1 = 1.10±0.02 $M_\odot$ and m_2 = 0.83±0.02 $M_\odot$. The high orbital inclination $i = 87.6^\circ \pm 0.1^\circ$ was confirmed by photoelectric observations of the secondary minimum. The mean observed U light curve shows additional light during the secondary minimum. The small eccentricity found by several authors from the light-curve analysis cannot be ruled out. The face-to-face position of the spots on the surface of both components in 1971 indicates the possibility of a mass transfer from the primary to the secondary component through a magnetic bridge connecting both active regions. Analysis of all available light curves suggests a random position of starspots and does not confirm the idea of active longitude belts. The absolute parameters of the binary together with maximal apparent V brightness set the distance of RT And to 83±2 pc, close to the Hipparcos value of 75±6 pc.

Key words: stars: binaries: eclipsing – stars: individual: RT And – stars: magnetic fields

1. Introduction

Active eclipsing binary RT And (BD +52°3383a, F8-G0 V + K1-3 V, $V_{max} \approx 8.9$) is RS CVn-like short-period (P = 0.62893 days) system.

The variability of RT And has been known since the beginning of the 20th century (Deichmueller, 1901; Zinner, 1915). The photographic light curve (LC) of RT And was obtained by Jordan (1929) and later by Payne-Gaposchkin (1946). The first photoelectric LCs of RT And were obtained in 1948 - 1950 by Gordon (1948, 1955). She found the LC to be variable and asymmetric in the secondary eclipse and noted that the primary minima occurred earlier than predicted. Wood & Forbes (1963) fitted the observed period decrease using the third order polynomial. Williamon (1974) interpreted the observed orbital period decrease by two period jumps caused by instantaneous mass exchange bursts. On the other hand, Albayrak et al. (1999) and Borkovits & Hegedüs (1996) explained the long-term orbital period decrease by a light-time effect (LITE) caused by the presence of one or two other bodies, respectively.

Dumitrescu (1973b, 1974) analyzed photometric LCs of RT And obtained in 1971 (Dumitrescu, 1973a) and found a slightly eccentric orbit with e = 0.08. He explained some characteristics of the LC by random mass loss from the primary component almost filling the corresponding Roche lobe and a hot spot on the secondary component. Milano et al. (1981) analyzed 10 available photoelectric LCs obtained up to 1978, derived mean photometric elements and proposed a "migration wave" caused by the spots with a period of about 22 years equal to the magnetic activity cycle. Zeilik et al. (1989a) explained the photometric distortion waves in the LCs by dark, circular starspots. They derived the temperature of the spotted region on the primary star to be roughly 1100-1200 K below that of the surrounding photosphere. The spotted region tends to appear in two active longitude belts near 90° and 270°. Analysis of good-quality LCs provided an orbital eccentricity e = 0.026. Zeilik's method and computer codes were used also by Heckert (1995, 1996 and 1998) to analyze his 1995 - 1997 observations. Monitoring of the LC of RT And from 1988 to 1992 was performed by Dapergolas et al. (1988, 1991, 1992 and 1994).

Photometric solutions of RT And V LCs led to a detached configuration with a smaller secondary component and an inclination angle close either to 82° (Payne-Gaposchkin, 1946; Mancuso et al., 1979c; Milano, 1981) or 88° (Dean, 1974; Dumitrescu, 1974; Milano et al., 1981; Budding & Zeilik, 1987; Zeilik et al., 1989a). Both solutions were also found by Arévalo et al. (1995) from analysis of the infrared J and K LCs. They argued in favour of the second solution. Comparison between the synthetic (from ATLAS atmosphere models) and observed B,V,J,H and K magnitudes gave effective temperatures of the components of 6000 K and 4900 K with an uncertainty of 125

Send offprint requests to: T. Pribulla

Table 1. U,B,V magnitudes and their standard errors (in parentheses) of comparison stars used by previous authors (see Table 7)

BD+52°	V	B	U	Sp.	Note
3375	9.392	10.557	12.249	K0	RZ And
	±2	±4	±12		
3377	8.783	10.297	12.93	–	
	±9	±3	±3		
3380	9.683	9.843	10.859	–	
	±6	±7	±12		
3382	10.060	10.134	10.526	F0	susp. var.*
	±6	±7	±18		
3383	7.244	7.243	7.116	B0	
	±1	±6	±19		
3384	10.12	10.25	10.96	–	adopted**
3385	9.818	10.264	11.157	A3	
	±6	±4	±4		

* Kukarkin, 1982, ** Heckert (1995)

K. The observed colours correspond to G0 V and K2 V spectral types.

Payne-Gaposchkin (1946) obtained the first radial velocity (RV) curves of both components and determined their G0 V and K1 V spectral types. Kron (1950) found a faint phase-dependent emission in Ca II H and K lines on the spectra obtained by S. Gaposchkin (Payne-Gaposchkin, 1946). Roman (Gordon, 1955) determined the F8 V spectral type of the primary component from the spectrum (taken at the phases 0.47 - 0.50). Further spectra used for the RV determination were obtained by Wang & Lu (1993) and Popper (1994). Their RV curves, however, differ in the semi-amplitude of the secondary component resulting in a different total mass of the binary. Gunn et al. (1996) published only a few RVs of both components. Arévalo & Lázaro (1999) found phase-dependent emission in H_α, H_β and Ca II infrared triplet related to an inhomogeneous distribution of active regions on the primary component. The rotational velocity of the primary component $v \sin i$ = 109 kms^{-1} determined by Huisong & Xuefu (1987) corresponds to a synchronous rotation.

Budding et al. (1982) analyzed low-dispersion IUE spectra. The detected emissions in Mg II H and K lines indicate a high degree of chromospheric activity. RT And is an X-ray source with L_X = 1.3 10^{30} erg s^{-1} (Dempsey et al., 1993). The system was not detected as a radio source ($L_R < 0.16$ mJy at λ = 6 cm, Drake et al., 1986).

Since RT And is quite bright, it was one of the targets of the Hipparcos astrometric mission. The resulting parallax π = 13.3 ± 1.1 mas (Popper, 1998) corresponding to the distance d = 75±6 pc is a crucial test of the correct determination of absolute parameters of RT And and constitutes the main impetus for the present study.

2. New photometry and minima times

Our photoelectric observations of RT And were obtained at the Skalnaté Pleso (SP) and Stará Lesná (SL) Observatories of the Astronomical Institute of the Slovak Academy of Sciences. The system was observed in 19 nights from August, 1997 to December, 1999. In both cases a single-channel pulse-counting photoelectric photometer installed at the Cassegrain focus of the 0.6m reflector was used. Observations at SP were carried out through the standard B, V and R filters using photomultiplier HAMAMATSU R 4457P sensibilised in the R passband. The standard U,B and V filters were employed at SL using photomultiplier EMI 9789 QB.

The integration time of one measurement was 10 seconds. BD+52°3384 and BD+52°3377 served as comparison and check stars, respectively. The magnitude differences between these stars reached about 0.04 mag in V, and 0.06 mag in B and U. These variations are rather higher than the standard errors of U,B,V magnitudes during individual nights. Therefore, the stability of these comparison stars must be checked by further observations.

The standard error of one observation during clear nights reached 0.015 mag in U, 0.009 mag in B and 0.008 mag in V and R passband. The rather large error in U is caused by the low brightness of both comparison stars in this passband.

The standard international U,B,V magnitudes were obtained from instrumental u,b,v magnitudes using the following transformations:

$$\begin{aligned} \mathrm{V} &= \mathrm{v} - k_V(\mathrm{b}-\mathrm{v}) \\ \mathrm{B}-\mathrm{V} &= k_{BV}(\mathrm{b}-\mathrm{v}) \\ \mathrm{U}-\mathrm{B} &= k_{UB}(\mathrm{u}-\mathrm{b}) \end{aligned}$$

The transformation coefficients k_V, k_{BV}, k_{UB} are determined by the observations of the standard stars in the Pleiades, Praesepe and IC 4665 open clusters. These observations are performed routinely every two or three months on both telescopes. R magnitudes are in the instrumental system.

For the differential extinction correction we have used the average seasonal extinction coefficients.

On two nights (Dec 17, 1999 and Jan 6, 2000) we have measured the brightness of all comparison stars used by previous authors (Table 7). BD+52°3384 served as a principal comparison star. Its U,B,V,R and I international magnitudes were published by Heckert (1995). The resulting U,B,V magnitudes (and standard errors) for these stars are given in Table 1.

Although BD+52°3375 was denoted in GCVS as variable star RZ And, Schmidt (1996) found it to be constant. According to our determination, its brightness was stable within the errors. BD+52°3382 was measured only on one night, hence its suspected variability cannot be ruled out.

U,B,V and R observation obtained in 1998 of RT And are shown in Fig. 1. During our 1997 - 1999 observations the UBVR LCs were quite stable. There is larger scatter of the observations in the secondary minimum than in other phases in all passbands. Individual observations can be obtained via ftp from `cdsarc.u-strasbg.fr`.

Our observations led to the determination of 17 minima times. We have calculated them separately for all three passbands using the Kwee and van Woerden's method (1956), parabola fit, tracing paper and center of mass method which were described in detail by Ghedini (1982). The computer code

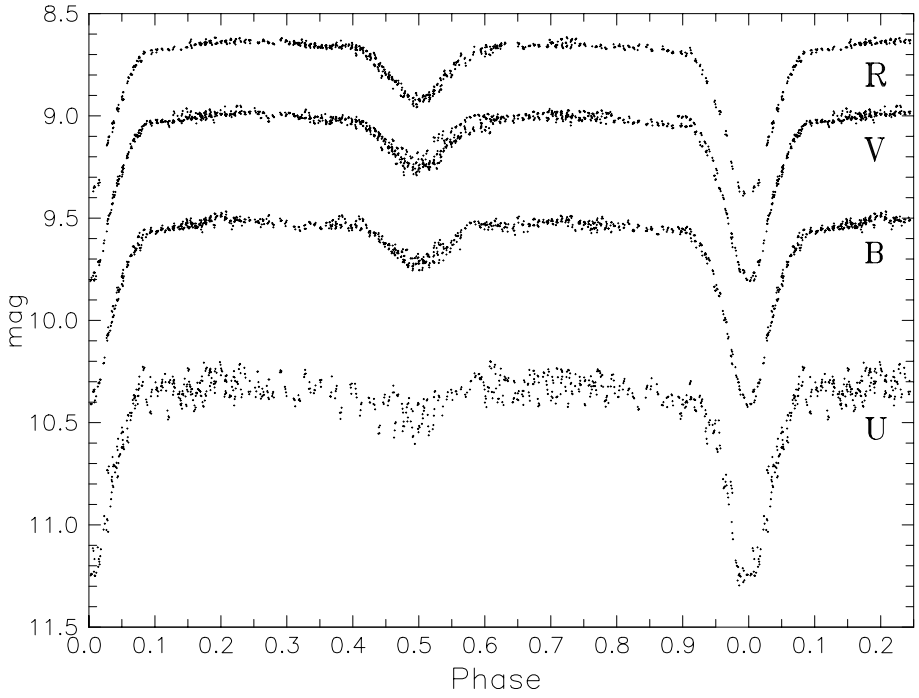

Fig. 1. 1998 U,B,V observations at the Stará Lesná Observatory and B,V,R observations at the Skalnaté Pleso Observatory.

was kindly provided by Komžík (1999). For computations we have used only observations around the primary and secondary minimum in the phase intervals ± 0.02 and ± 0.04, respectively. This approach diminished the influence of the minima asymmetries as described by van't Veer (1973). Moreover, these parts of the minima were found to be sufficiently symmetric.

Minima observed in 1997 and 1998 were already published (Pribulla et al., 1999b). The times of three primary and six secondary minima obtained in the 1999 season are listed in Table 2. Differences between the instances of the minima obtained by the individual methods and filters are usually lower than 0.001 days except two minima with insufficiently covered descending branches (Sep 11 and Dec 17, 1999). The differences are caused by the fact that some of the applied methods are far more sensitive (e.g., Kwee and van Woerden, 1956) to asymmetries of the minima than others. The scatter of minima visible in the (O-C) diagram is 0.003 days. Hence the influence of the asymmetries on the instants of the minima is unimportant. For the further study we have taken the parabola fitting method which is relatively insensitive to the minima asymmetries.

3. The orbital period analysis

For the analysis of period changes we have gathered all available photographic and photoelectric minima times from literature. Minima times determined from visual estimates were omitted. Older times of minima were taken from Williamon (1974), Bakos & Tremko (1981) and Rovithis-Livaniou et al. (1994). Recent minima times were taken from IBVS. The weights 1 and 5 were accepted for the minima times determined from the photographic and photoelectric observations, respectively. The averages calculated from minima times in different passbands were used. Altogether 169 minima times (41 photographic and 128 photoelectric) listed in Table 3 were used for further analysis. Two photographic and three photoelectric minima times deviating too much from the general trend were omitted. They are listed under the line at the end of compilation of the photographic and photoelectric minima.

Detected differences in the relative position of the secondary minima with respect to the expected photometric phase 0.5 were explained by an eccentric orbit. Milano (1981) found them to be highly variable and concluded that eccentricity is only the result of numerical artifice. On the other hand, Zeilik et al. (1989a) found from the LC analysis small eccentricity $e = 0.026 \pm 0.013$.

The displacement of the secondary minimum can be calculated in the first approximation (for small eccentricities, and inclination $i \approx 90^\circ$) by the well known relation:

$$\Delta T = \mathrm{Min\ II} - \mathrm{Min\ I} - \frac{P}{2} = \frac{2Pe\cos\omega}{\pi}, \qquad (1)$$

where Min II and Min I are times of consecutive secondary and primary minima, respectively. Parameter ω is the length of the periastron of the *primary* component. The displacement vanishes for $\omega = 90^\circ$ and 270°. Before the beginning of the spectroscopic observations analyzed in Sect. 4 only five secondary minima times were published. Ten secondary minima times fall within the range of the spectroscopic observations (1984-94). If we accept the spectroscopic elements: $e = 0.011 \pm 0.004$ and $\omega = 73^\circ \pm 26^\circ$ (Table 6), the relation (1) provides $\Delta T = 0.0012 \pm 0.0018$ days. The scatter of the minima times is about 0.003 days. Therefore an orbital eccentricity cannot be inferred from the secondary minima displacements. Thus we will treat primary and secondary minima together.

In our opinion the primary and secondary minima are most probably displaced and scattered in the (O-C) diagram by the presence of spots. These shifts simulate small orbital eccen-

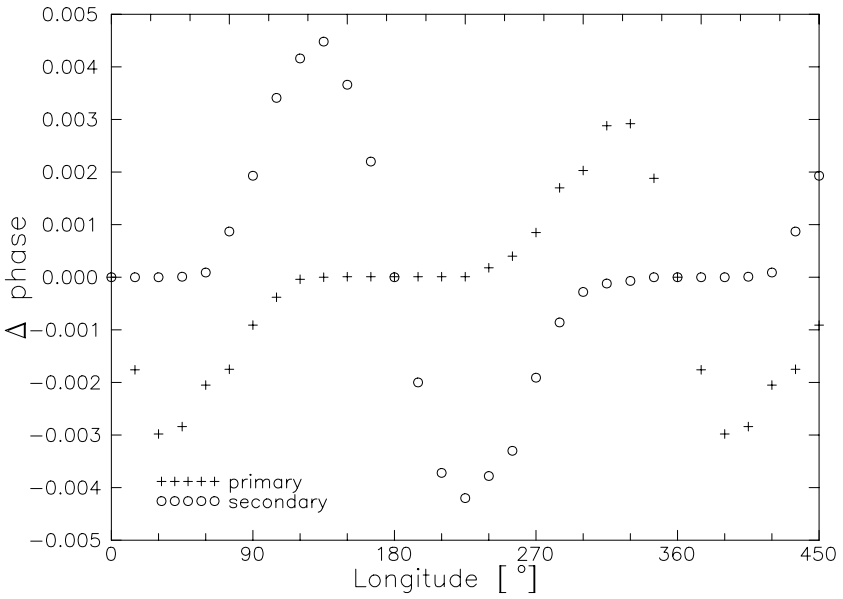

Fig. 2. Theoretical shifts of the primary and secondary minima caused by a dark circular spot on the primary component

Table 2. New times of the primary (I) and the secondary (II) minima

JD_{hel}	Obs.	Type	Filter	Method				
2 400 000+				P	CM	KW	SI	PL
51417	SP	I	B	.33616	.33607	.33593	.33621	.33681
			V	.33574	.33597	.33606	.33614	.33542
			R	.33516	.33536	.33535	.33540	.33516
51426	SP	II	V	.45424	.45368	.45354	.45376	.45294
			R	.45496	.45436	.45429	.45453	.45348
51433	SL	II	V	.37323	.37391	–	.37658	.37436
51434	SL	I	B	.31722	.31717	.31716	.31716	.31718
			V	.31733	.31739	.31738	.31782	.31733
51436	SP	II	B	.51930	.51966	–	.51959	.51841
			V	.51836	.51818	–	.51894	.51841
			R	.51786	.51859	–	.51913	.51868
51498	SL	I	B	.46800	.46792	.46793	.46808	.46828
			V	.46808	.46816	–	.46827	.46841
51508	SP	II	R	.21660	.21652	–	.21564	.21706
51511	SP	II	R	.36132	.36169	.36155	.36162	.36140
51530	SL	II	V	.22803	.22826	–	.22155	.22106

Methods: P - parabola fitting, CM - center of mass, KW - Kwee & van Woerden (1956), SI - sliding integrations, PL - polygonal line

tricity detected both spectroscopically and photometrically. We have computed theoretical displacements of the primary and secondary minima caused by a typical starspot r = 30° and k = 0.95 positioned on the primary component (see Sect. 5.4). The results of computations for several longitudes of the spot are shown in Fig. 2.

Due to the month-to-month variations in the spots parameters, the displacements cancel out on times scales of several months to years and contribute to an additional scatter of data in the (O-C) diagram.

3.1. Causes of the orbital period change

A linear ephemeris (4) was applied to construct the (O-C) diagram (Fig. 3). There are three possible interpretations of the observed data:

3.1.1. Two sudden period changes

Williamon (1974) interpreted the observed period decrease by two period jumps (around 1938 and 1964) caused by an instantaneous mass exchange between the components. To verify this possibility we have fitted the data by a broken line consisting of three linear parts:

$$\begin{aligned} \mathrm{Min\,I} &= JD_0 + PE + \tfrac{1}{2}Q_1|E-E_1| \\ &\quad + \tfrac{1}{2}Q_2|E-E_2|, \end{aligned} \tag{2}$$

where E_1 and E_2 are the epochs, Q_1 and Q_2 are the relative changes of the period during the first and the second period jump, respectively. JD_0 and P are the averages of the linear ephemerides during the first and the third part. For RT And a weighted least squares fitting by the relation (2) provides for $E \leq$ –6580:

Table 3. The average times of the primary (I) and secondary (II) minima in JD^*_{hel} (JD_{hel} - 2 400 000)

JD^*_{hel}	Type	Ref.	JD^*_{hel}	Type	Ref.	JD^*_{hel}	Type	Ref.	JD^*_{hel}	Type	Ref.
photographic minima											
20105.385	I	1	24286.534	I	3	24795.341	I	4	25912.324	I	3
20122.363	I	1	24434.340	I	4	24831.191	I	4	26000.376	I	3
20144.380	I	1	24446.284	I	4	24832.444	I	4	26176.473	I	3
20168.271	I	1	24490.313	I	4	24842.505	I	3	31435.608	I	5
20173.303	I	1	24686.535	I	4	24949.425	I	3	33230.576	I	50
20175.188	I	1	24732.448	I	4	25020.491	I	3	38288.432	I	52
22931.810	I	2	24751.322	I	4	25322.379	I	3	38644.407	I	53
22935.584	I	2	24756.346	I	4	25515.468	I	3	41605.412	I	54
22940.615	I	2	24761.383	I	4	25588.423	I	3	20005.417	I	1
22941.870	I	2	24769.555	I	4	25698.486	I	3	34979.645	I	51
22984.640	I	2	24778.359	I	4	25754.462	I	3			
photoelectric minima											
32443.7820	I	5	41141.8885	I	14	43725.5303	I	25	48858.5397	II	42
32758.8760	I	5	41143.7755	I	14	43732.4483	I	25	48861.3686	I	42
32763.9080	I	5	41167.6730	I	14	43880.2460	I	26	49734.3232	I	43
32775.8580	I	5	41194.7197	I	14	44173.3267	I	56	49972.3730	II	44
32787.8070	I	5	41197.8650	I	14	44851.3141	I	28	49973.3144	I	44
32804.7870	I	5	41218.6181	I	14	45630.5587	I	29	49981.4914	I	45
32865.7930	I	5	41227.4219	I	15	45673.3256	I	30	50000.3592	I	44
33175.8560	I	5	41230.5675	I	15	46298.4807	I	31	50001.3001	II	44
33587.8050	I	5	41232.4536	I	15	46988.4186	I	32	50004.4459	II	45
33627.4284	I	6	41261.3875	I	15	47015.4610	I	33	50682.4319	II	55
33837.4940	I	5	41300.3803	I	16	47044.3916	I	34	50708.5333	I	55
33918.6240	I	5	41508.5563	I	17	47082.75694	I	35	50709.4780	II	55
33920.5110	I	5	41598.4911	I	17	47381.4981	I	36	50964.5073	I	47
35066.4220	I	5	41619.2458	I	18	47756.3385	I	37	51041.5496	II	55
35454.4731	I	7	41627.4228	I	17	47758.5390	II	37	51066.3941	I	55
37958.8731	I	8	41886.5418	I	17	47759.4832	I	37	51076.4564	I	48
37987.8061	I	8	41905.4092	I	19	47760.4256	II	37	51103.5007	I	48
37999.7552	I	8	41924.2795	I	18	47763.5711	II	37	51142.4937	I	55
38227.4290	I	9	41932.4547	I	20	47803.5094	I	38	51150.35516	II	55
38651.3280	I	10	41947.5490	I	20	47806.3397	II	38	51160.4162	II	55
38778.6862	II	8	41952.5796	I	20	47817.3456	I	39	51417.3357	I	46
39390.3209	I	11	41956.3540	I	20	48125.5202	I	38	51426.4546	II	46
39422.3936	I	11	42011.3852	II	17	48126.4657	II	38	51433.3732	I	46
39429.3122	I	11	42317.3611	I	21	48130.5518	I	38	51434.3173	II	46
39441.2630	I	11	42329.3092	I	17	48132.4386	I	38	51436.5185	II	46
39739.3740	I	12	42330.5675	I	17	48133.3849	II	38	51498.4680	I	46
40115.4755	I	13	42338.4240	II	17	48506.3373	II	40	51508.2166	II	46
40161.3878	I	56	42339.3710	I	17	48510.4262	I	41	51511.3613	II	46
40190.3175	I	56	42367.3586	II	17	48511.3688	II	41	51530.2280	II	46
40196.2900	II	56	42385.2832	I	17	48512.3124	I	41	33477.4790	I	49
40197.2368	I	56	42717.3586	I	22	48514.5131	II	41	44820.4880	I	27
40200.3815	I	56	43044.3992	I	23	48600.3641	I	40	51179.3440	I	48
40439.3750	I	13	43381.5065	I	24	48646.2748	I	40			

References: 1 - Zinner (1915), 2 - Jordan (1929), 3 - Nijland (1931), 4 - Sternberk (1927), 5 - Gordon (1955), 6 - Lenouvel (1951), 7 - Lenouvel (1957), 8 - Dean (1974), 9 - Pohl & Kizilirmak (1964), 10 - Pohl & Kizilirmak (1966), 11 - Kristenson (1967), 12 - Kizilirmak & Pohl (1969), 13 - Pohl & Kizilirmak (1970), 14 - Williamon (1974), 15 - Dumitrescu (1973a), 16 - Pohl & Kizilirmak (1972), 17 - Mancuso et al. (1978), 18 - Kizilirmak & Pohl (1969), 19 - Baldinelli et al. (1973), 20 - Murnikova & Lemeshchenko (1981), 21 - Baldinelli & Ghedini (1976), 22 - Pohl & Kizilirmak (1976), 23 - Patkos (1980), 24 - Ebersberger et al. (1978), 25 - Mancuso et al. (1979b), 26 - Pohl & Gulmen (1981), 27 - BBSAG No. 56, 28 - Pohl et al. (1982), 29 - BAAVSS No. 60, 30 - Pohl et al. (1985), 31 - Pohl et al. (1981), 32 - BBSAG No. 84, 33 - Keskin & Pohl (1989), 34 - BAAVSS No. 70, 35 - Caton et al. (1991), 36 - Hanžl (1990), 37 - Rovithis-Livaniou et al. (1994), 38 - Dapergolas et al. (1991), 39 - BAAVSS No. 73, 40 - Hanžl (1994), 41 - Dapergolas et al. (1992), 42 - Dapergolas et al. (1994), 43 - BBSAG No. 108, 44 - Müyesseroğlu et al. (1996), 45 - Albayrak et al. (1996), 46 - present paper, 47 - Borkovits & Biro (1998), 48 - Agerer & Hübscher (1999), 49 - Ashbrook, (1952), 50 - Latrob (1950), 51 - Azarnova (1955), 52 - Obůrka (1964), 53 - Obůrka (1965), 54 - Ahnert (1973), 55 - Pribulla et al. (1999a), 56 - Bakos & Tremko (1981)

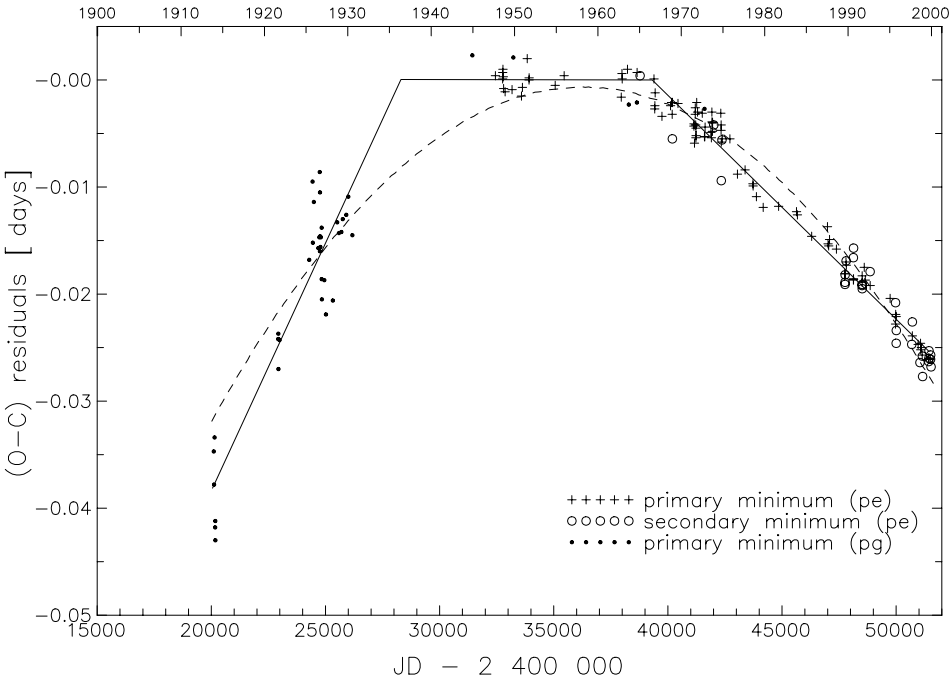

Fig. 3. (O-C) diagram from the linear ephemeris (4) for all photographic and photoelectric minima, quadratic fit and the broken-line fit

$$\begin{array}{lll} \text{Min I} = 2\,432\,443.8008 & +0.62893358\ E \\ & \pm16 \qquad\quad \pm9 \end{array} \tag{3}$$

for –6580 $\leq\ E\ \leq$ 10930:

$$\text{Min I} = 2\,432\,443.7816 + \ 0.62893067\ E, \tag{4}$$

and finally for $E\ \geq$ 10930 we have:

$$\text{Min I} = 2\,432\,443.7961 + \ 0.62892935\ E. \tag{5}$$

The standard errors (given in Eq. (3)) are the same for all three ephemerides. The unweighted sum of squares of residuals for the three linear fits is 0.000706 d^2. The moments of the jumps correspond to JD 2 428 300 ± 330 (May 1936) and JD 2 439 320 ± 320 (Jul 1966). The first sudden period change $\Delta P/P$ = –(4.63±0.16) 10^{-6} was larger than the second one $\Delta P/P$ = –(2.10±0.16) 10^{-6}. These period changes could be explained by mass transfer bursts from the primary to the secondary component. Assuming a conservative case and mass points approximation and accepting the total mass of the binary m_1+m_2 = 1.96 M$_\odot$ and mass ratio q = 0.75 (see Sect. 4), we have determined the transfered mass as Δm = (5.18±0.18) 10^{-6} M$_\odot$ and Δm = (2.35±0.18) 10^{-6} M$_\odot$ during the first and the second period jump, respectively.

3.1.2. Continuous period decrease

The weighted least squares fitting of the data by a parabola provided the following quadratic ephemeris:

$$\begin{array}{lll} \text{Min I} = 2\,432\,443.7792 & +0.62893124 & E \\ & \pm3 \qquad\quad \pm3 & \\ & -4.66 & 10^{-11}\ E^2 \\ & \pm11 & \end{array} \tag{6}$$

From the quadratic coefficient we have $\Delta P/P = -(8.60 \pm 0.22)\ 10^{-8}$ year^{-1}. On the same assumptions as in the broken-line fit we got the mass transfer rate Δm = (9.64±0.25) 10^{-8} M$_\odot$ year^{-1}. The total shortening of the orbital period since the first minimum (December 1913) sums up only to 0.365 seconds. The unweighted sum of squares of residuals for the parabola fit is 0.0016159 d^2. It is important to note that the data are much better explained by a third order polynomial ($\Sigma(O-C)^2$ = 0.0010911 d^2). Therefore there must be a further effect affecting the data. The deviation of the parabola from the data is best visible from JD 2443000 to 2447000.

To explain these differences we have assumed that the times of the primary minima follow a quadratic ephemeris and are deviated by the LITE, so the minima times can be computed as follows:

$$\begin{aligned} \text{Min I}\ &= JD_0 + PE + QE^2 + \\ &+ \tfrac{a_{12}\cdot\sin i}{c}\left[\tfrac{1-e^2}{1+e\cos\nu}\sin(\nu+\omega) + e\sin\omega\right], \end{aligned} \tag{7}$$

where $a_{12}\sin\ i, e, \omega$ are orbital elements, ν is the true anomaly of the binary orbit around the center of the mass of the triple system, $JD_0 + PE + QE^2$ is the quadratic ephemeris of the minima in an eclipsing binary and c is the velocity of the light. To obtain the optimal fit and corresponding elements of the light-time orbit including errors, we have used the differential corrections method (see also Chochol et al., 1998). The resulting optimal ephemeris of the binary as well as the elements of the eccentric orbit of the eclipsing pair around the mass center of the triple system are given in Table 4. The corresponding fits are shown in Fig. 4.

Since the minimum mass of the third body, calculated from $f(m_3) = 3.1\ 10^{-5} M_\odot$ and the mass of the binary, is only $0.05^{+0.007}_{-0.010}$ M$_\odot$ its contribution to the LC is negligible. More-

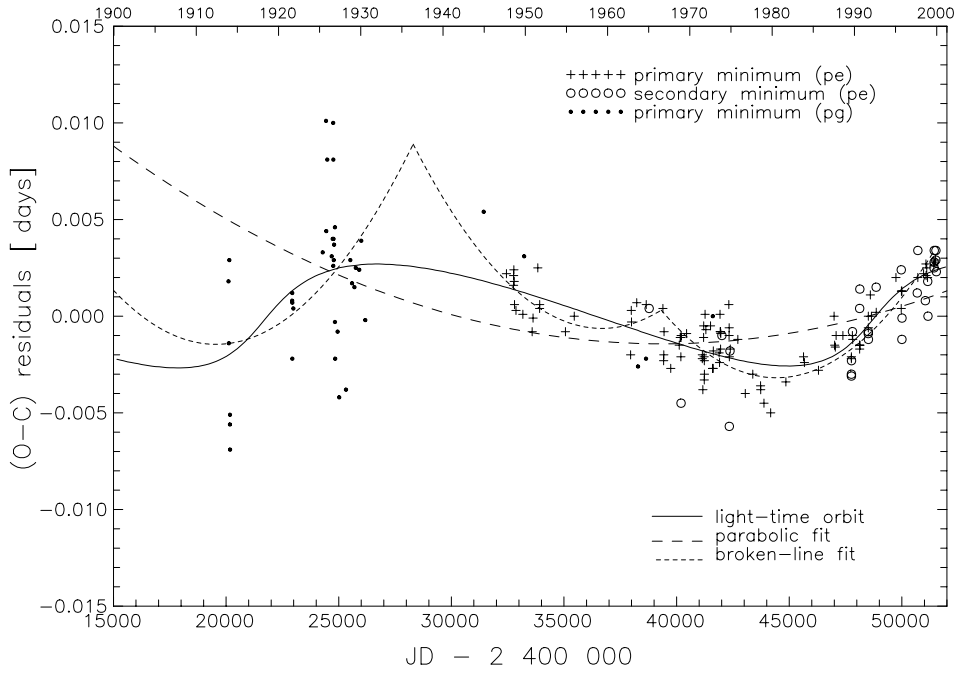

Fig. 4. (O-C) diagram from the optimal quadratic ephemeris for the light-time effect fit corresponding to the elements in Table 4. The parabolic fit corresponds to ephemeris (6), the broken-line fit to ephemerides (3)–(5)

over, the predicted total change of the systemic velocity of the binary is about 0.56 km s^{-1}, which is well under the present precision of the RV observations of RT And.

3.1.3. Light-time effect caused by the fourth body

The overall period decrease could also be explained by the LITE caused by the presence of the fourth body. Even if it is the case, the available data ($\approx$ 85 years) cover only part of the possible orbit. Therefore the orbital period of such a body is very uncertain. The 110 and 108 years orbits derived by Borkovits & Hegedüs (1996) and Albayrak et al. (1999) have to be taken with caution.

Borkovits & Hegedüs (1996) explained the (O-C) residuals from the linear ephemeris of the binary (for data till JD 2448500) by the presence of the two bodies with 51 years and 110 years orbits. Since their fit explains data very well, we have applied weighted differential corrections for the LITE caused by two other bodies for our set of data. We have assumed (not fixed) linear ephemeris for the eclipsing pair. The differential corrections converged slowly since the period of the fourth body is very uncertain. Although most parameters did not change for longer interval of time, we got a longer period of the fourth body $P_4 \approx 115$ years and $e_4 = 0.7 \pm 0.1$. The unweighted sum of residuals reached 0.0005805, not a large improvement for as many as 12 free parameters. The method and its application to a quadruple system SW Lac is described in Pribulla et al. (1999c).

3.2. Discussion

The data can be represented by two sudden period changes in 1936 and 1966, a continuous period change combined with the LITE due to the presence of the third body (Fig. 4) or by the LITE caused by the third and fourth body. The parabolic fit alone cannot explain the data well. The unweighted sum of squares of residuals is nearly equal for the broken-line fit and the continuous period change combined with the LITE. The broken line fit has, however, only 6 free parameters. It is clear that the period jump is only a mathematical approximation of a fast period change lasting for a finite time. Due to simplicity and clarity, we will use the broken-line ephemerides for the calculation of the orbital phases in our paper.

Period jumps could be explained by eruptive mass transfer bursts from the primary to the secondary component. RT And is a system with well separated components. Therefore it is not feasible to assume a flow of matter between the components through the inner Lagrangian point L_1. There is also the

Table 4. The third body elements with corresponding ephemeris of the binary system and their standard errors (σ). T_{super} and T_{infer} are the times of the superior and inferior conjunction of the third body, respectively

Element			σ
$P_{third\ body}$	[days]	27000	3700
e		0.56	0.13
ω	[°]	351	20
T_0	[JD]	2 448 500	1000
$a_{12} \sin i$	[AU]	0.55	0.11
$f(m_3)$	[$M_\odot$]	0.000031	0.000020
T_{super}	[JD]	2 446 700	1500
T_{infer}	[JD]	2 451 200	1800
JD_0	[JD]	2 432 443.7798	0.0006
P_{binary}	[days]	0.62893139	$8\ 10^{-8}$
Q	[days]	$-5.34\ 10^{-11}$	$0.33\ 10^{-11}$
$\sum$(O-C)^2	[days^2]	0.0006268	–

possibility that the matter flows from the primary to the secondary component through the open magnetic lines of force. Since the involved mass is quite large, this process should be detected observationally. Unfortunately, photometric observations do not cover the epochs of jumps. The first photoelectric LC after the period jump in 1966 was obtained by Dumitrescu (1973a) in 1971. Our solution of this LC (Sect. 5.4) suggests the presence of two spots on the primary and secondary component in a face-to-face position, which indicates the possibility of an intermittent mass transfer from the primary to the secondary component through a magnetic bridge connecting both active regions, responsible for the period jump.

The same mechanism could explain the continuous period decrease. Another possibility is the magnetic braking process. Hall et al. (1980) determined the minimum magnetic surface field, 526 Gauss, required to produced the observed long-term period decrease $\Delta P/P$ = (–1.17±0.06) 10^{-7} year^{-1}.

The long-term period decrease could also be explained by the LITE caused by a fourth body. Due to the fact that only part of the hypothetical fourth body orbit is covered by observations, any computation of orbital elements requires extrapolation, so it is highly speculative and problematic. Our observations cover a longer time interval than the data of Borkovits & Hegedüs (1996) and Albayrak et al. (1999), so it is not surprising that the fourth body orbital period $P_4 \approx 115$ years is longer than in previous studies. The orbital period of the third body depends on the LITE fit of the fourth body. The advantage of the combined third and fourth body LITE solution is that it does not require any complicated physical process to explain the observational data. The presence of these bodies could be tested by precise radial velocity measurements or speckle interferometry.

As in the case of AW UMa (Pribulla et al., 1999b) it is impossible to decide which interpretation of the period change is true for RT And. The problem will be resolved by future observations.

4. Radial velocity curves and their solution

4.1. Previous studies

The RVs of both components of RT And were determined in four studies. Three of them were also devoted to the computation of the absolute parameters of the system.

The first RV curves of both components of RT And, based on medium dispersion (not given in the original paper) spectra taken in December 1944, were published by Payne-Gaposchkin (1946). We have found the following spectroscopic elements using these data: K_1 = 130 ± 4 km s^{-1}, K_2 = 204 ± 8 km s^{-1}, V_0 = 22.8 ± 2.9 km s^{-1}, e = 0.062 ± 0.028, ω = 240° ± 24°. These values together with i = 82.7° determined by Payne-Gaposchkin (1946) from photographic LC analysis yield: m_1 = 1.51 ± 0.18 M$_\odot$ and m_2 = 0.97 ± 0.11 M$_\odot$. The RV data of Payne-Gaposchkin (1946) are shifted about +20 km s^{-1} with respect to later spectroscopic studies since the measurements of RT And were not accompanied by those of standard stars. Hence we have not used the data in the further study.

Table 5. Corrected RVs from Gunn et al. (1996)

JD$_{hel}$ 2 400 000+	Phase	RV_1 [km s^{-1}]	RV_2 [km s^{-1}]
49643.6882	0.883	64.5	–
49644.7140	0.514	16.2	–
49646.6109	0.530	19.5	–
49647.6430	0.171	-118.3	146.3
49650.7486	0.109	-93.7	127.8
49654.6285	0.278	-125.9	158.0
49655.6222	0.858	98.6	-136.6
49657.6348	0.058	-60.4	98.5

The RVs published by Payne-Gaposchkin (1946) suffer from systematic shift (+20 km.s^{-1}) caused by the fact that the measurements of RT And were not accompanied by those of standard stars. The lines of the secondary component were detected only on 5 spectra. Hence we have not used the data in the further study.

Wang & Lu (1993) presented RV observations of RT And taken in 1984-1985 and found K_1 = 131.4±0.5 km s^{-1}, K_2 = 168.4±1.4 km s^{-1}, V_{01} = -1.0±0.4 km s^{-1}, V_{02} = 5.0±1.2 km s^{-1}. They performed a joint solution of their RVs and UBV LCs taken from Mancuso et al. (1979b) and determined the basic parameters of the system using the W&D program as follows: $m_1 = 1.045 \pm 0.013$ M$_\odot$, $m_2 = 0.812 \pm 0.009$ M$_\odot$, $i = 81.20° \pm 0.16°$.

Further high-quality spectra of RT And were obtained by Popper (1994) in 1989-1993. He derived the RVs by the advanced cross-correlation CCF method using theoretical corrections for rotational velocities, line strength ratios, line separations and proximity effects and determined K_1 = 135.4±0.6 km s^{-1}, K_2 = 185.1±1.0 km s^{-1}, V_{01} = 4.8±0.5 km s^{-1}, V_{02} = 4.7±0.8 km s^{-1}. Adopting $i = 88.4° \pm 0.4°$ from Zeilik et al. (1989a), he determined the masses of the components as $m_1 = 1.24 \pm 0.03$ M$_\odot$ and $m_2 = 0.91 \pm 0.02$ M$_\odot$.

The last spectroscopic observations aimed at the determination of the RVs were obtained in 1994 by Gunn et al. (1996). The part of their paper devoted to RT And is, however, full of errors and misinterpretations. The ephemeris of Popper (1994) quoted on page 153 of their paper was not used for the calculation of epochs in their Table 3 since it gives times of observations in the future. The epochs and phases were actually calculated by the ephemeris given in Strassmeier et al. (1993). Three values of RVs in Table 3 of Gunn et al. (1996) were erroneously assigned to the cooler (secondary) component even though it was obscured in phases 0.514 and 0.530. Their Fig. 13 is also confused. Although their conclusions about a change of the orbital period and apparent inconsistency of spectroscopic observations with Popper's values are erroneous, their RVs are suitable for computation of the spectroscopic orbit. Correct HJDs and RVs are given in Table 5.

4.2. Spectroscopic elements

The RV data published by Wang & Lu (1993), Popper (1994) and Gunn et al. (1996) were determined by the cross-correlation

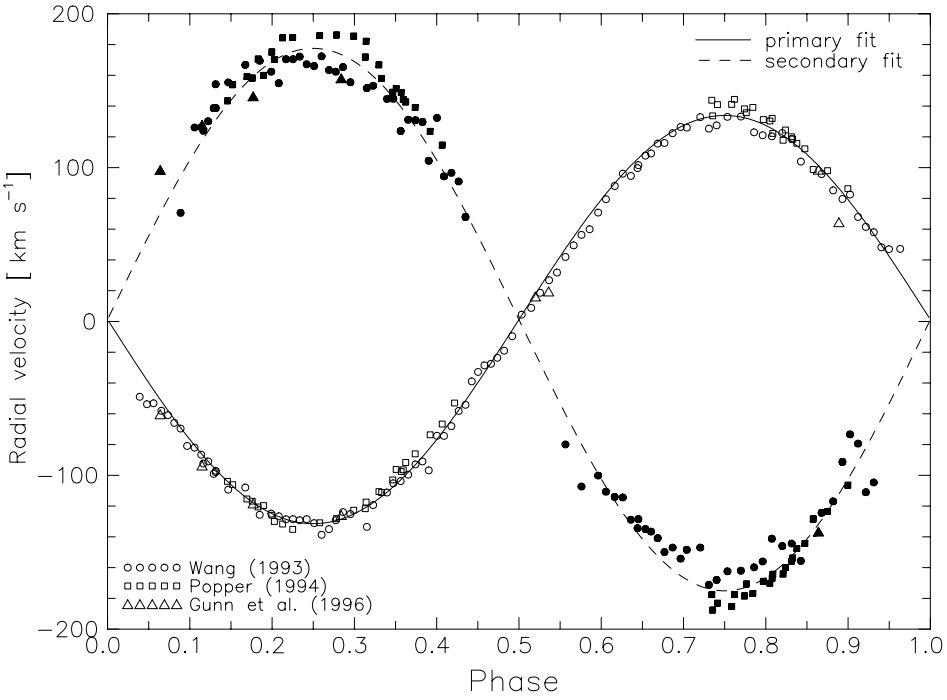

Fig. 5. The RVs of the primary and secondary component and their best fits for an eccentric orbit. The phases were computed from the optimal linear ephemeris (5). The empty and filled symbols denote RVs of the primary and secondary component, respectively

function method. We used all three sets for determination of spectroscopic elements.

Since the RV data were obtained over an interval of more than 10 years (1984 - 1994), when the orbital period of the binary was quite stable (see Sect. 3), we have not fixed the orbital period found from photometry. First we have assumed zero eccentricity and simultaneously fitted RVs of the primary and secondary component by the differential correction method assuming two mass points. This preliminary fit provided the ratio of variances of the observed RVs of the primary and secondary component $\sigma^2_{pri}/\sigma^2_{sec}$ = 0.493. In the second optimization we have used this value for weighting the dataset of the secondary component. The individual RVs were not weighted. The resulting spectroscopic elements in case of eccentric orbit are given in Table 6 (solution (1)) and the best fits are shown on Fig. 5. The spectroscopic elements for the circular orbit are within the errors of parameters obtained for eccentric orbit.

From Fig. 5 one can see that the RVs of the primary component do not differ much between particular studies. On the other hand, the semi-amplitude of RVs of the secondary components obtained by Popper (1994) is larger than that of Wang & Lu (1993). This is partly caused by blending of the profiles of the primary and secondary component in the cross-correlation function in lower dispersion data of the latter authors (see Popper, 1994). Part of the problem, however, can be connected with an uneven distribution of the surface brightness on the secondary component. This effect could also be ascribed to the presence of the spots on the secondary component markedly shifting the light center of the star from the gravity center. The differences in RVs of the secondary component observed by Wang & Lu (1993) could be caused by the presence of a dark spot on the hemisphere of the secondary component facing the observer during the primary minimum. Above all, RVs of the primary component are lower than expected after the secondary eclipse, indicating the presence of dark spots on the primary component, too.

Table 6. The best spectroscopic elements of RT And in mass points approximation (1) and with proximity and eclipse effects included (2). The standard errors σ are given in parentheses

Element		(1)	(2)
JD_0	[HJD]	2432443.80(5)	–
P	[days]	0.6289292(2)	–
T_0	[HJD]	2432443.77(5)	–
e		0.011(4)	0.010(3)
ω	[°]	73(26)	26(20)
V_0	[km.s^{-1}]	1.2(5)	0.5(3)
K_1	[km.s^{-1}]	132.6(7)	132.0(6)
K_2	[km.s^{-1}]	176.2(1.1)	178.3(1.2)
$a_1 \sin i$	[AU]	0.00766(4)	0.00763(2)
$a_2 \sin i$	[AU]	0.01018(6)	0.01031(3)
$m_1 \sin^3 i$	[M$_\odot$]	1.094(21)	1.119(15)
$m_2 \sin^3 i$	[M$_\odot$]	0.823(15)	0.828(11)
q		0.752(22)	0.740(4)
$\Sigma(O-C)^2$	[km^2.s^{-2}]	21328.4	22094.7

As expected, the resulting systemic velocity V_0 and semi-amplitudes of the RV curves K_1 and K_2 are between the values obtained by Popper (1994) and Wang & Lu (1993). The same is valid for the resulting masses of the components: $m_1 \sin^3 i$ = 1.097±0.016 M$_\odot$ and $m_2 \sin^3 i$ = 0.825±0.017 M$_\odot$. The mass ratio is q = 0.752 ± 0.016. Although these values do not supersede previous determinations they pose a reasonable estimate of the absolute parameters of the components. It is interesting to note that the ephemeris for the superior conjunctions of the

primary (primary minimum) is within the errors of the linear ephemeris (5) found from photometric data and also valid in the interval of spectroscopic observations.

To ascertain the reality of the small eccentricity e = 0.026±0.013 (ω = 264±13°) determined by Zeilik et al. (1989a), we have reanalysed RVs by the W&D code taking into account the Rossiter and proximity effects (solution (2) in Table 6). We have assumed photometric elements for the high-inclination solution (Table 8). This resulted in even smaller eccentricity e = 0.010±0.003 with $\omega = 26 \pm 20°$. Although the eccentricity exceeds three σ limit, the orientation of the orbit is inconsistent with the orientation found from the LC analysis by Zeilik et al. (1989a).

5. Light-curve analysis

5.1. Historical light curves

RT And is a system displaying pronounced long-term variations of the LC. The last paper dedicated to this analysis was published by Zeilik et al. (1989a). Since then many new photoelectric observations have been published which together with this paper enlarge the number of V LCs to 27. Only a small part of the photometry was performed in the U passband. Near-infrared filters (R and/or I) were employed by Zeilik et al. (1982, 1988), Gordon et al. (1990) and Heckert (1995, 1996 and 1998). The list of available LCs is given in Table 7.

Unfortunately, part of the published LCs were not given in tabular form. These LCs were scanned from original papers and saved as bitmap pictures. Then we have carefully determined the pixels coordinates appropriate to the centers of the symbols. Although the symbols clumped in some phases, we were able to reconstruct the original shape. For every scanned figure as many as eight pixel coordinates of points with known phase and Δ mag (or intensity) were taken. The least squares method of optimization of these data provided the rotational and scaling matrix for transformation from pixels to phases and magnitudes. The mean standard error of the recovered data did not exceed 0.002 in magnitudes and 0.005 in phases for any figure. We have found small differences in data between repeated phases in the same figure e.g., in the paper of Zeilik et al. (1982).

Scanned data were rephased so that the primary minimum coincides with phase zero. Since part of the LCs were published in intensities, the observers used different comparison stars and a large part of observations was published only in the instrumental system, we could not transform the data to the international UBVRI system. We obtained a more or less homogeneous dataset by transforming the observed magnitude differences between the variable and comparison star to intensities. The LCs were normalized to the brighter maximum. Although this procedure obliterated intrinsic changes in the maximum (total) brightness of the system, the overall shape of the LCs was preserved. Published observations exceeding 500 in one passband, were used to calculate about 300 normal points. Large number of individual observations in a few cases (e.g., LC 11) exceeded both computer memory and arrays dimensioning in the W&D code.

Our observations were processed by the same way. All available LCs are shown in Fig. 6. The original observations were additionally provided by Heckert (1999).

It is clearly seen that the U and B LCs exhibit the most pronounced variations especially during the secondary eclipse. The sense of the asymmetry of the minimum is observed to be variable. The LC maxima differ in both possible ways. The most significant LC changes registered in October-December 1974 (LCs 9 and 10) by Mancuso et al. (1979a) suggest that the time scale of the changes of the positions and sizes of the spots cannot be longer than one month. On the other hand, our 1997-9 observations of RT And show only small LC variations in spite of quite a good time coverage.

5.2. Composite light curves

The LC of RT And is highly variable due to the presence of spots. The effect of maculation is most pronounced in the U and B passbands. Hence, it is difficult to find a "clean" LC. On the other hand, infrared LCs are almost unaffected.

Zeilik et al. (1989a) found that the deformation of all published LCs from 1920 - 1989 can be explained by the presence of one dark spot positioned on the primary component around quadrature longitudes i.e., the spot affects only one maximum. Therefore the phases around the other (brighter) maximum are virtually clean. We have taken phases from preceding to following minimum (the adjacent half of the LC) for the composite U,B and V LCs. The clean maxima were also tested for symmetry. The shift of the phase of maximum light with respect to quadrature was taken as a simple indicator of the symmetry. We have found the phase shift 0.07 to be a good compromise between the number of usable LCs and asymmetry. A few individual low intensity points which deviated too much from the composite LCs were removed. The resulting clean U,B and V LCs are displayed in Fig. 7.

The symmetry of the resulting composite LCs is noteworthy. Since the coverage of some phases (e.g., the ascending branch of the secondary eclipse of the U passband) was scanty, we have folded the data around phase 0.5. This was also applied to R, I, J and K LCs. The resulting (direct plus folded) data were used to construct normal points. The number of individual points included into one normal point varied from 4 for infrared LCs to 19 in V passband so that the number of resulting normal points was about 200 for each LC.

5.3. Simultaneous solution of the composite light and radial velocity curves

In most previous LC analyses of RT And (Zeilik, 1989a; Heckert, 1995, 1996, 1998; Arévalo et al., 1995) the LCs in different passbands were treated separately leading to different geometrical elements for each passband. The mass ratio was usually either assumed from spectroscopy or both components were approximated by spheres.

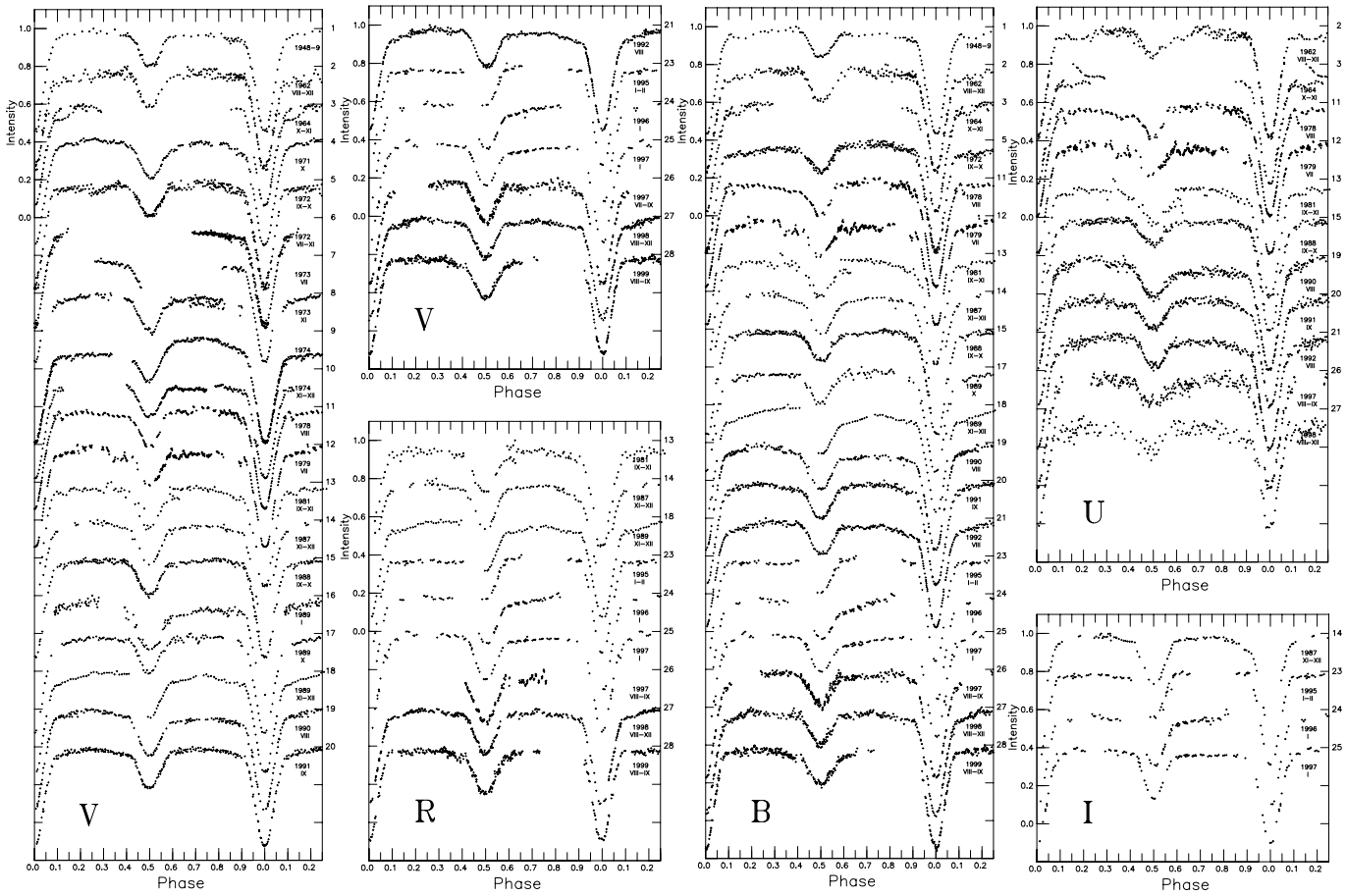

Fig. 6. Historical U,B,V,R and I light curves of RT And

Since we had at our disposal all RVs and LCs in 7 passbands, we decided to take advantage of the simultaneous LC and RV curve fitting (see Wilson, 1979) and multifrequency analysis.

The U,B,V,R,I,J and K LCs and RVs were analyzed using the synthetic LCs and the differential corrections code developed by Wilson & Devinney (1971) (W&D). We have used the 1992 version (Wilson, 1992) of his program. The particular numbers of individual photometric observations coming into one normal point were used as weights. The RV data were not weighted individually. For each LC and RV curve the values of σ were carefully evaluated as described by Wilson (1979). The initial values of photometric and spectroscopic parameters of RT And were taken from Wang & Lu (1993). Mode 2 of the W&D code appropriate for detached binaries was employed assuming synchronous rotation and zero eccentricity. For the computation of luminosities we have used the approximate atmospheric models option of the W&D program (Carbon-Gingerich atmospheres). Coefficients of gravity darkening g_1 = g_2 = 0.32 (Lucy, 1967) and bolometric albedo A_1 = A_2 = 0.5 (e.g., Rucinski, 1969) were fixed as appropriate for the convective envelopes. The limb darkening coefficients were interpolated from Table 1 of Al-Naimiy (1978). The spectral type - effective temperature calibrations differ markedly: Johnson (1966) gives for F8V T_{eff} = 6000 K and for G0V T_{eff} = 5900 K, while Lang (1992) gives T_{eff} = 6200 K and T_{eff} = 6030 K. Therefore we have fixed the mean temperature of the primary component at two boundary values 6200 and 5900 K.

Arévalo et al. (1995) found that the infrared LCs can be fitted almost equally well by two sets of photometric parameters for $i = 82°$ and $i = 87°$. The analysis of the eclipse morphology, evolutionary models prediction as well as χ^2 favour the high inclination solution. These solutions differ mainly in the ratio of radii of the primary and secondary component.

To validate all possibilities we have performed four solutions – two for high inclination and two for low inclination. In each case we have run the differential correction code as long as output corrections were smaller than the errors of the elements. The resulting geometric elements do not differ significantly for the solutions with different temperatures. Therefore, we present only the lower temperature solution in Table 8. Fits corresponding to the high and low inclination solution differ only slightly (Fig. 8). The most marked difference is the constant-light phase during the secondary minimum due to the total eclipse of the secondary component. For the lower inclination the eclipses are partial. The weighted sum of squares of the residuals favors the high inclination solution.

We have also checked the possibility of a small orbital eccentricity by analysis of the mean LCs. This approach is justified

Table 7. Sources of published photoelectric and CCD light curves. The numbering of the light curves is the same as in Fig. 6. The filters not given in capitals mean the observations were published in the instrumental photometric system. The diameters of telescopes employed are given in cm

Data set	Date	Filters	Comparison BD+52....	Reference	Observatory Telescope	Note
1	1948-9	bv	3382, 3384	Gordon (1955)	Li - 30,91	s
2	1962, Aug 6 - Dec 28	UBV	3382, 3384	Dean (1974)	SD - 61	o
3	1964, Oct 3 - Nov 28	UBV	3382, 3384	Dean (1974)	ML - 41	s
4	1971, Oct 1-8, 1971	V	3383	Dumitrescu (1973a)	On - 65	o
5	1972, Sep 2 - Oct 5	BV	3382, 3385	Murnikova & L. (1981)	OM - 50	o
6	1972, Jul 9 - Nov 5	v	3377, 3380	Mancuso et al. (1979a)	Te - 40	o
7	1973, Jul 21 - 22	v	3377, 3380	Mancuso et al. (1979a)	Te - 40	o
8	1973, Nov 23 - 28	v	3377, 3380	Mancuso et al. (1979a)	Te - 40	o
9	1974, Oct 8 - 18	v	3377, 3380	Mancuso et al. (1979a)	Te - 40	o
10	1974, Nov 18 - Dec 4	v	3377, 3380	Mancuso et al. (1979a)	Te - 40	o
11	1978, Aug 2-11	ubv	3384, 3377	Mancuso et al. (1979b)	Te - 50	n
12	1979, Jul 15-24	ubv	3377, 3384	Milano et al. (1986)	Te - 50	n
13	1981, Sep 20 - Nov 16	ubvr	3383	Zeilik et al. (1982)	CP - 61	s
14	1987, Nov 11 - Dec 12	bvri*	3384	Zeilik et al. (1988)	CP - 61	s
15	1988, Sep 26 - Oct 19	UBV	3384, 3377	Dapergolas et al. (1988)	Kr -120	s
16	1989, Jan 15-21	v*	3384	Zeilik et al. (1989a)	CP - 61	s
17	1989, Oct 3-7	BV	3384, 3377	Dapergolas et al. (1991)	Kr -120	s
18	1989, Nov 10 - Dec 12	bvr*	3384	Gordon et al. (1990)	CP - 61	s
19	1990, Aug 21-29	UBV	3384, 3377	Dapergolas et al. (1991)	Kr -120	s
20	1991, Sep 10-16	UBV	3384, 3377	Dapergolas et al. (1992)	Kr -120	s
21	1992, Aug 23-27	UBV	3384, 3377	Dapergolas et al. (1994)	Kr -120	s
22	1990-4	JK	3375	Arévalo et al. (1995)	Td -150	o
23	1995, Jan 18 - Feb 20	BVRI	3384	Heckert (1995)	ML - 61	o
24	1996, Jan 2-8	BVRI	3384	Heckert (1996)	ML - 61	o
25	1997, Jan 7-11	BVRI	3384	Heckert (1998)	ML - 61	o
26	1997, Aug 21 - Sep 17	UBVR	3377, 3384	present paper	SP,SL - 60	n
27	1998, Aug 15 - Dec 2	UBVR	3377, 3384	present paper	SP,SL - 60	n
28	1999, Aug 26 - Sep 14	UBVR	3377, 3384	present paper	SP,SL - 60	n

CP - Capilla Peak, Kr - Kryonerion, Li - Lick, ML - Mount Laguna, On - Ondřejov, OM - Odessa (Majaky), SD - San Diego, SL - Stará Lesná, SP - Skalnaté Pleso, Td - Teide, Te - Teramo

Notes: o - original tabular data, s - scanned and transformed, n - normal points constructed from tabular data,
- CCD photometry

because the orientation of the orbit between 1978 - 1997 (Zeilik et al., 1989a; Heckert, 1998) varies only $\pm 19^\circ$. The optimal orientation and eccentricity of the orbit were found by fixing of ω with the step of 5° and running differential corrections code for each initial value. The improvement of the solution was rather small (the reduction of the $\sum w(O-C)^2$ is about 1%). The resulting eccentricity is e = 0.005±0.002 and ω = 270±5°agrees well with the value determined by Zeilik et al. (1989a). Unfortunately there is only scanty information about the orbital eccentricity in the LCs because for ω = 270° (and ω = 90°) the displacement of the secondary minimum vanishes. In this case, the primary and secondary minima are symmetric and of different width.

The observations show marked asymmetries of the minima (see Fig. 6). Moreover, the predicted differences in the width of minima are very small for e = 0.005.

The reliable determination of such a small orbital eccentricity is complicated by the presence of the photospheric spots.

Although the mass functions of the third and/or fourth body (see Sect. 3) are rather small, we have tried to look for their contribution to the mean LCs. The resulting third light is very small and inconsistent between the filters (l_{3B} = 0.0064±0.0019, l_{3V} = 0.0008±0.0018, l_{3R} = 0.0115±0.0026 and l_{3I} = 0.0045±0.0041). The third light is higher than the standard error of single observation of average weight only in the R passband (σ_R = 0.004). Hence, the presence of other bodies cannot be concluded from the LC analysis.

It is remarkable that the optimal elements satisfactorily fit all LCs. The only significant departure from the fit occurs for both the low and high inclination solution in the U passband. The U LC shows additional light during the secondary minimum caused either by extra-photospheric matter as indicated by the presence of the emission components in the Ca II H and K lines (Kron, 1950) or a lower temperature of the secondary component T_{eff} = 4650 K than expected for the combination of the two stars of G0V and K2V spectral types. It is also possible that the U passband excess is caused by an inadequacy

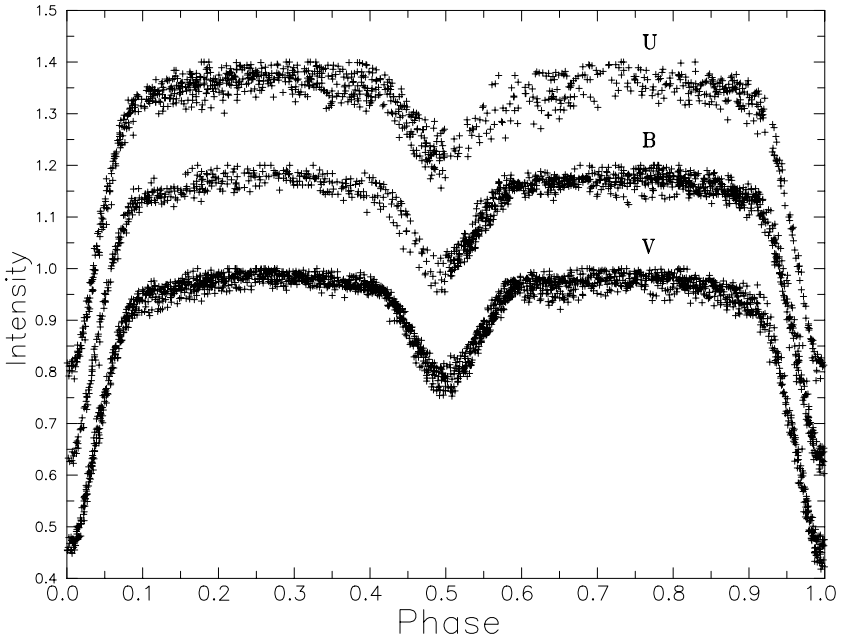

Fig. 7. The composite clean U,B and V LCs of RT And

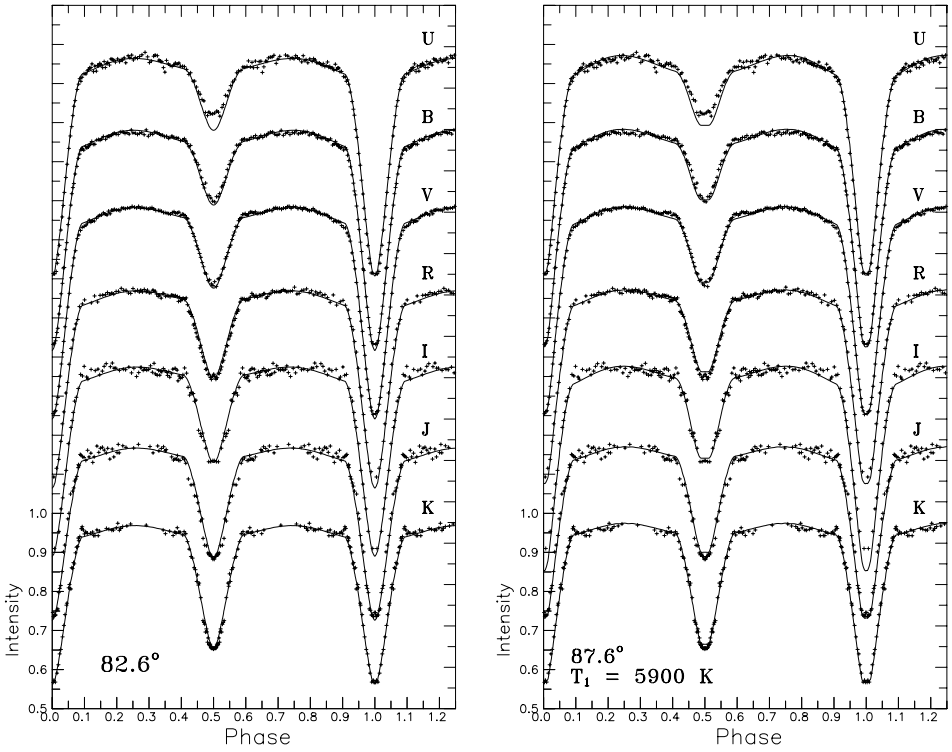

Fig. 8. U,B,V,R,I,J and K normal points and corresponding fits for the low (left) and high (right) inclination solution

of the Carbon-Gingerich atmospheres model used in the W&D program.

The best photometric and spectroscopic elements are given in Table 8. Corresponding 3D surfaces for both the low and high inclination solutions and the orbital phase 0.25 are shown in Fig. 9.

To choose between the two possible inclinations we have performed an observational test. The secondary minimum of RT And was additionally observed on November 25 and 28, 1999 in the R passband at the SP observatory (these data were not included in the LC analysis). In spite of variable observational conditions the observations favor the total eclipses corresponding to the high inclination solution (see Fig. 10). This solution was used in the spot analysis.

5.4. Analysis of individual spots

The best photometric elements obtained on the assumption of a circular orbit were used as clean parameters for the star-spot modeling. This was performed only for U,B,V and R LCs, since

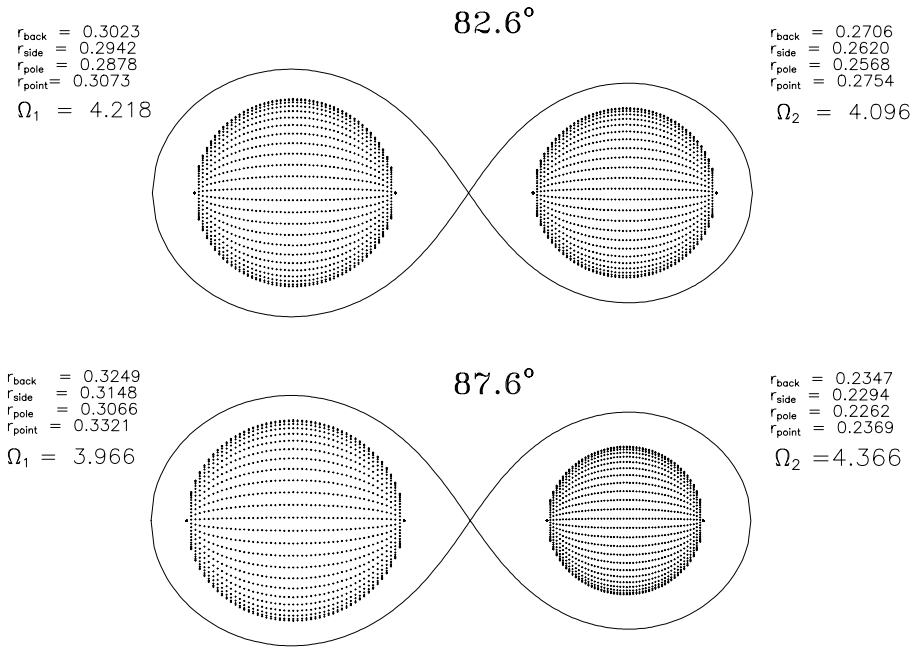

Fig. 9. 3D surfaces, fractional radii and surface equipotentials corresponding to the low (upper) and high (lower) inclination solution.

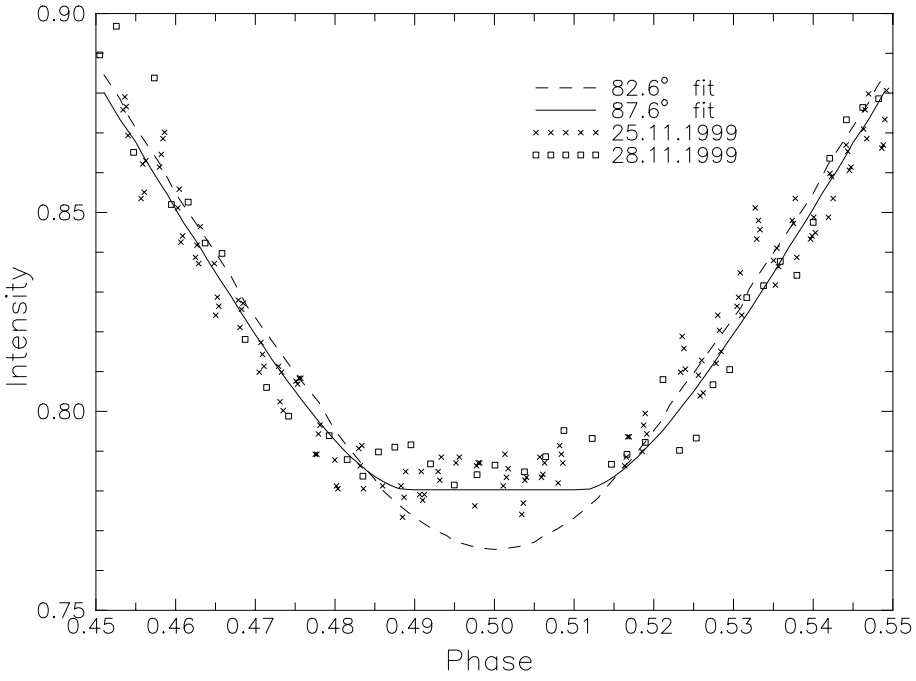

Fig. 10. R passband secondary minimum observations and fits for the low and high inclination solution

in the infrared (I,J and K) we have only a few LCs and they contain only scanty information about spots.

The preliminary longitudes of the spots were determined from the residuals of the particular U,B,V and R LCs from the high inclination solution in Table 8 ($i = 87.6°, T^1_{eff}$ = 5900 K). The residuals from the low inclination solution differ markedly only during eclipses. Dark spot regions display themselves in residuals as depressions. Since the system is well detached, the center of the depression corresponds to the longitude of the spot on the surface. The longitudes are counted in the direction of the orbital motion from the L_1 point throughout our paper. The positions of the spots were determined using the methods of Ghedini (1982) for determination of minima times (see Sect. 2). The resulting positions of the spots are given in Table 9. Their uncertainties fall within 5 - 10°. Some information about the radius of a spot can be extracted from the width of the depression in the residual curve. The radius of the spot is always smaller than the width of the depression in degrees. In case of a spherical star, a spot of radius R_{spot} placed on the equator is visible by an observer on Earth over the phase interval $\approx 180° + 2R_{spot}$ (if the spot is not eclipsed by the other component). This simple method, however, does not enable us to determine if a particular spot is located on the primary or secondary star. In spite of the simplicity of this method the results are in most cases in

Table 8. Spectroscopic and photometric elements and their standard errors (σ) - i - inclination; $q = m_2/m_1$ - mass ratio; Ω_1, Ω_2 - surface potentials; r_1, r_2 - volume mean fractional radii calculated from the surface potentials; T_1, T_2 - polar temperatures. $\sum w(O-C)^2$ is the weighted sum of squares of residuals for all light and RV curves. Parameters not adjusted in the solution are denoted by a superscript "a"

Element		Low **i**		High **i**	
			σ		σ
A [R$_\odot$]		3.839	0.021	3.865	0.021
V_0 [km.s^{-1}]		0.8	0.6	0.6	0.6
K_1 [km.s^{-1}]		133.7	1.2	131.9	1.0
K_2 [km.s^{-1}]		172.7	1.5	178.8	1.3
m_1 [M$_\odot$]		1.083	0.018	1.128	0.018
m_2 [M$_\odot$]		0.838	0.014	0.832	0.014
i [°]		82.56	0.05	87.57	0.11
q		0.7742	0.0013	0.7374	0.0027
Ω_1		4.218	0.004	3.966	0.002
Ω_2		4.096	0.004	4.366	0.003
r_1		0.2948	0.0001	0.3159	0.0002
r_2		0.2635	0.0005	0.2303	0.0004
T_1 [K]		5900^a	–	5900^a	–
T_2 [K]		4643	16	4651	3
	U	0.8348	0.0002	0.8824	0.0001
	B	0.8285	0.0002	0.8776	0.0001
	V	0.8044	0.0002	0.8593	0.0001
$L_1/(L_1+L_2)$	R	0.7717	0.0003	0.8341	0.0001
	I	0.7407	0.0004	0.8097	0.0001
	J	0.6796	0.0005	0.7601	0.0002
	K	0.6258	0.0005	0.7146	0.0002
M_1^{bol} [mag]		4.43	–	4.26	–
M_2^{bol} [mag]		5.71	–	5.98	–
log g_1 [cm.s^{-2}]		4.37	–	4.32	–
log g_2 [cm.s^{-2}]		4.35	–	4.46	–
$\sum w(O-C)^2$		0.08048	–	0.08003	–

agreement with the spot longitudes determined by the more sophisticated method of Zeilik et al. (1989a).

The preliminary longitudes determined by this method were used as an input parameter for the W&D code (used the same manner as described above). Since the 1992 version of the code does not include the atmospheric models for temperatures lower than 4500 K we have used the black-body approximation in cases of such cool spots. The geometric elements obtained for the high inclination solution and the temperature of the primary component T_{eff} = 5900 K were fixed. First we improved the longitude of the spot. Then, for observations in more than one colour, we also tried to determine the temperature factor and radius of the spot. Unfortunately, an area of a spot is highly correlated with its temperature. On the other hand, the latitude of a spot is highly correlated with its radius and could be reliably determined only for eclipsed spots. In spite of this, for every spot we have explored the reasonable range of radii for the best fit.

Eker (1999) has shown that the current present precision of the photometric observations does not allow reliable determination of the latitudes of spots. Since the scatter of individual LCs is quite large, we assumed the latitude 90°(equator) in cases when the spots were not eclipsed. In most cases we found two spots, but we were not able to distinguish if the spots were located on the primary or secondary component. This is the case for spots located around longitudes 90° and 270°. Therefore, for the sake of simplicity we assumed the location of both spots to be on the primary component. This is justified also by time-resolved spectroscopy of RT And showing the primary to be the more active component.

As can be seen from Fig. 6, several LCs do not have sufficient phase coverage. This is the case for LCs 3,6,7,8,10, and 26. LCs 13, 14 are of inferior quality. The rest of the LCs were used for the determination of the spot parameters. The resulting spot parameters determined by the W&D method are given in Table 9. The average standard errors of the spot longitudes, spot radii and temperature factors are 5°, 5° and 0.001, respectively.

The results, given in Table 9, show quite good agreement with the residuals fitting and the Zeilik et al. (1989a) method. There is, however, inconsistency of the spot positions in cases where we needed two spots to explain the behaviour of the LC properly. This is the case of LCs 9, 19 and 28 (denoted by superscript b in the residuals fitting method). These cases could also be explained by one large dark zone extending over $\approx 120°$ in longitude.

For the LC 4 of Dumitrescu (1973a), which was considered as a textbook case of eccentric orbit by Zeilik et al. (1989a), we were able to distinguish the location of spots on both stars. As shown on Fig. 13, the spots are located on the facing hemispheres of the primary and secondary component at latitudes of about 45°. The magnetic lines of these spots were probably interconnected indicating formation of a bridge between the components, which enables mass transfer along magnetic lines. It is interesting to note that this configuration was detected five years after the possible period shortening of the system around 1966.

In cases when the LC was sufficiently described by one spot we have tried to put the spot on the secondary component. The fit as well as sum of squares of residuals did not change much: e.g., the solution of the LC 23 gives the sum of squares of residuals for the spot on the primary and the secondary components 0.0133 and 0.0136, respectively. On the other hand, for the LC 24 the solution is unique. The spot must be located on the primary component, since the decrease of the brightness of RT And occurs around the secondary minimum when the secondary component is eclipsed.

The LC solution was improved by a spot on the secondary component in the case of the LC 21 taken by Dapergolas et al. (1994).

5.5. Star-spots cycle length

The longitude of the spots has been checked for periodicity by the use of the phase dispersion minimization method (see Stellingwerf, 1978). The best periodicity P = 140 days (in the range 10 - 10000 days) gives low significance and a not-meaningful phase diagram for longitude. Zeilik et al. (1989a)

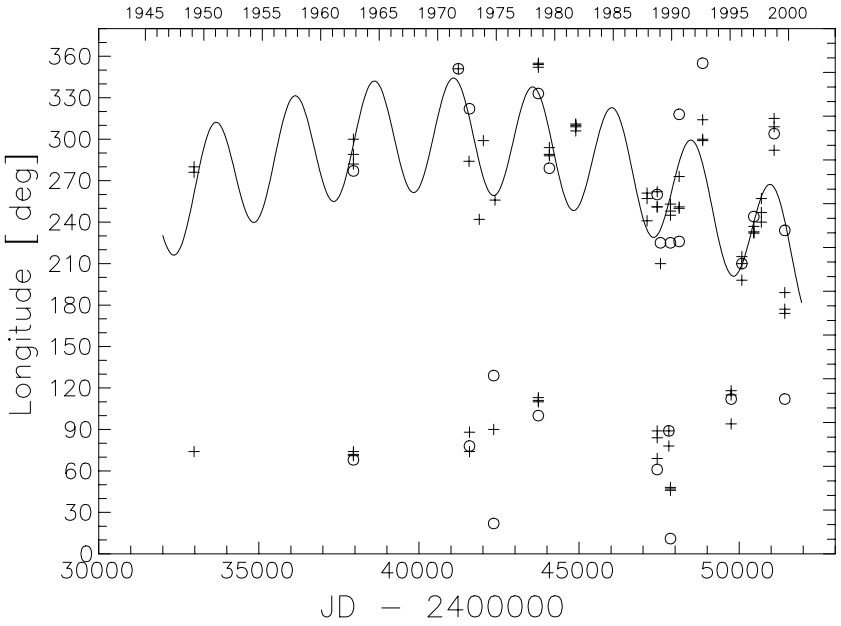

Fig. 11. Longitudes of the spots (from Table 9) for residuals fitting (crosses) and W&D method (circles) and optimal fit of the spot longitudes in the "belt" around 270°

found that the spot tend to occur around quadrature longitudes (90° and 270°) forming active longitude belts. New and more extensive parameters of the spots do not confirm this hypothesis (see Fig. 11) although the occurrence of the spots in the vicinity of quadrature longitudes is visible. Latest LCs, however, show spots close to $l = 180°$ and so both "belts" seem to converge into one wide "belt". The positions of the spot within the "belt" around 270° seem to be periodic. The optimal fit, shown in Fig. 11, obtained by the differential corrections method assuming quadratic trend combined with a sine wave, gives the period 6.8±0.5 years. During this possible cycle the spot oscillates around quadrature position.

There is also the possibility that the extent of the spot area or total light blocked by the spots is periodic, resembling the activity of the Sun. In spite of the indeterminacy of the spot radii and temperature factors simultaneously (in several cases) we have evaluated the total luminosity blocked by the spot. This can be estimated from the Stefan-Boltzmann law. The surface of a circular spot on a spherical star is:

$$S_{spot} = 4\pi r_{star}^2 \sin^2(R_{spot}/2), \tag{8}$$

where R_{spot} is the angular radius of the spot as seen from the center of the star with the radius r_{star}. For the evaluation of the total disturbance of the LC we can introduce a dimensionless factor β defined as the ratio of the luminosity blocked by spots and the total luminosity an unspotted binary. In the case of n_1 spots on primary and n_2 spots on secondary we can get:

$$\beta = \frac{\sum_{i=1}^{2}\sum_{j=1}^{n_1,n_2} r_i^2 \sin^2(R_j/2) T_i^4 (1-k_j^4)}{r_1^2 T_1^4 + r_2^2 T_2^4}, \tag{9}$$

where T_1 and T_2 are the mean temperatures of the unspotted components, k_j are temperature factors and R_j are the radii of j-th spot and r_j are radii of the components. The resulting spot factors obtained for individual LCs are given in Table 9. The spot factor also reflects an amount of the deformation of the particular LC. For clean LC it is zero. The resulting spot factors were checked for periodicities using the PDM method (Stellingwerf, 1978) in the range 10 - 10000 days. The best period in this range is 77.8 days. This period, however, does not give a reasonable phase diagram. The spot factor β and magnitude of the LC disturbance changes quite rapidly - e.g., LCs 17 and 18. This indicates a fast variability of the spot extent on the time scales of months even weeks. The disturbance of the LC by spots does not obey any strict periodicity.

6. Basic parameters and the distance to the system

The distance to RT And is one of most controversial parameters. The most precise parallax π = 13.3 ± 1.1 mas, resulting from the Hipparcos mission, places the system at the distance d = 75±6 pc. The distances determined from the absolute dimensions and temperatures of the components of RT And vary largely: Wang & Lu (1993) combined computed bolometric luminosities of the components M_{V1} = 4.14 and M_{V2} = 5.65 with incorrect values of interstellar absorption A_V =1.2 mag and observed visual magnitude of the system outside eclipses V = 8.55 and found very low distance to the system d = 50 pc. On the other hand, Arévalo et al. (1995) used higher semi-amplitudes of the RVs from Popper (1994) and V_{max} = 8.99. The observed (V-K) and (V-J) did not show any interstellar extinction. Therefore, it was neglected leading to the distance 103 pc.

The radiative flux of RT And and few other binaries (SZ Psc, LX Per and UV Psc) is markedly below the value expected from the intrinsic B-V index and Hipparcos distance (Popper, 1998). The author ascribes this discrepancy to surface irregularities and spots blocking part of the outgoing flux in the visual region. Hence, the visual magnitudes do not correspond to observed colour indices or spectral types determined from the spectroscopy shifting such systems to a higher distance.

Table 9. Spots longitudes determined using residual fitting. Spot longitude (l), radius (R_{spot}) and temperature factor (k) determined by the W&D method. β denotes the spot factor defined by Eq. (9). The last column gives spot longitudes in previous studies

Data	JD	Residuals fitting					W&D				Others	Reference
set	2 400 000+	U	B	V	R	Note	l	R_{spot}	k	β		
1	32978		280	276								
			74									
2	37954	72	71	74			68	20	0.919	0.0135	239	Zeilik et al. (1989a)
		289	282	300			277	30	0.970			
4	41229			199			30 s	35	0.790	0.0251	270	Zeilik et al. (1989a)
				351			351	35	0.943			
5	41579		74	88			78	25	0.949	0.0123	83	Banks (1991)
							322	35	0.983			
6	41567			284								
7	41885			242							286*	Zeilik et al. (1989a)
8	42012			299							286*	Zeilik et al. (1989a)
9	42333			90		b	22	40	0.952	0.0353	95	Zeilik et al. (1989a)
							129	40	0.950			
10	42377			256								
11	43727	111	113		110		100	50	0.986	0.0125	112	Zeilik et al. (1989a)
		355	354	352			333	35	0.985			
12	44074	288	289	294			279	20	0.951	0.0046		
13	44896	309	306	311	310						143	Zeilik et al. (1989a)
14	47126		261	257	241						260	Zeilik et al. (1989a)
15	47442	84	89	69			61	60	0.987	0.0163		
		262	251	251			260	20	0.937			
16	47544			210			225	80	0.982	0.0240	252	Zeilik et al. (1989a)
17	47804		89	78			89	25	0.979	0.0032		
18	47856		47	46	48		11	70	0.982	0.0244		
			245	253	248		225	35	0.959			
19	48128	273	251	250		b	226	30	0.965	0.0131		
							318	15	0.878			
21	48859	68	52	52			314 s	30	0.900	0.0266		
		314	300	299			355	90	0.986			
23	49752		94	115	118		112	40	0.981	0.0072	117	Heckert (1995)
24	50087		215	210	198		210	25	0.948	0.0075	216	Heckert (1996)
25	50457		237	232	233		244	25	0.959	0.0060	240	Heckert (1998)
26	50695	240	257	247								
27	51094		309	292	315		304	35	0.986	0.0041		
28	51426		177	189	174	b	234	25	0.942	0.0163		
							112	25	0.944			

$*$ - light curves 7 and 8 combined
b - belt (consists of two or more spots)
s - spot on the secondary component

The distance determined indirectly from absolute parameters is affected by three crucial parameters: mean effective temperatures corresponding to outgoing fluxes, apparent magnitude and interstellar extinction. The first parameter depends substantially on spectral type-T_{eff} calibration and absolute dimensions determination. The apparent magnitude is usually varying in RS CVn systems, therefore one should use apparent magnitude and spectral type from the same epoch. On the other hand, interstellar extinction is of little importance since these systems are closer than $\approx$150 pc, unless some additional extinction is caused by circumstellar matter. This can be, however, found from the observed colour indices.

Although RT And is quite close to the galactic plane (l = 108.06°, b = -6.93°) the extinction in its direction is negligible (Lynds, 1962). For a reasonable estimate of the apparent visual magnitude we can take V = 8.9 obtained by Murnikova & Lemshchenko (1981). The reasonable range for the effective temperature of the primary is 5900 - 6200 K. The bolometric luminosities of the components for the lower and higher inclination solution differ. Using the bolometric corrections for each component from Lang (1992) and zero extinction, the resulting distance to RT And in the case of lower and higher inclination is 79.1 pc and 82.9 pc for T_{eff} = 5900 K or 90.3 pc and 93.0 pc for T_{eff} = 6200 K. The uncertainties of the distances were

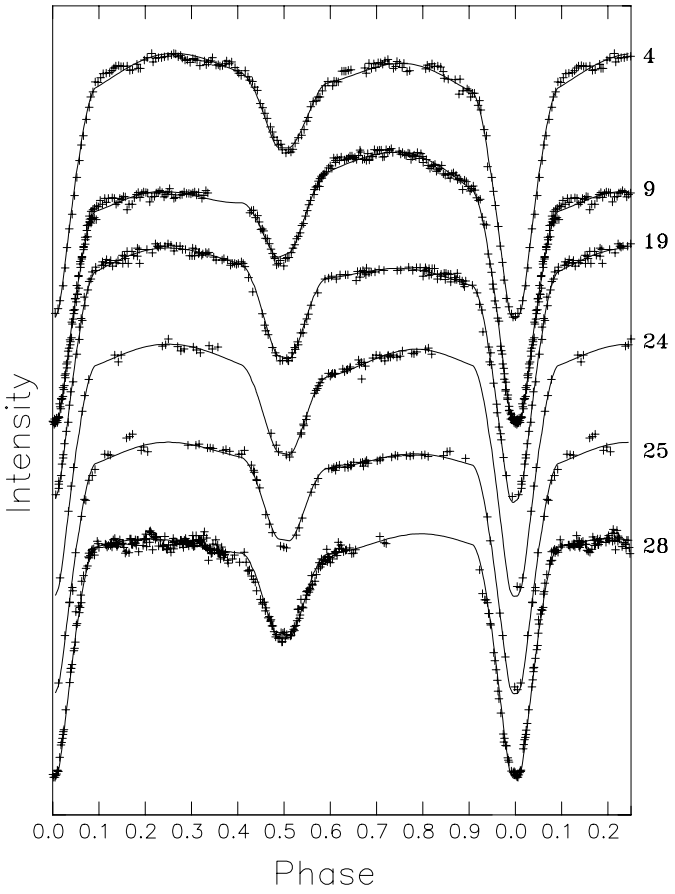

Fig. 12. V passband spot fits for the high inclination solution. The numbering of the light curves corresponds to Table 7

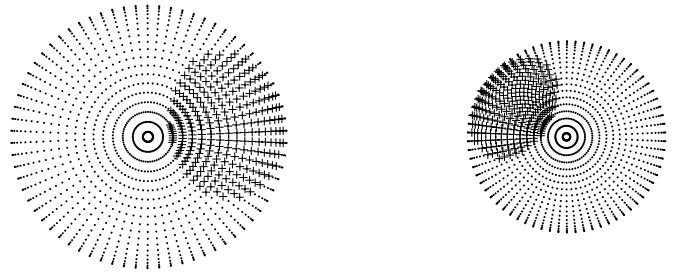

Fig. 13. Polar view of RT And with spots corresponding to the LC of Dumitrescu (1973a). The figure was produced by Binary Maker 2.0 (Bradstreet, 1993)

estimated from the errors of the semi-major axis, inclination and mass ratio to be about ± 2 pc.

The distance d = 79.1 pc obtained for T^1_{eff} = 5900 K, T^2_{eff} = 4643 K for the low inclination solution is within the error of the Hipparcos value 75$\pm$6 pc. The photometric analysis supports the high inclination solution with d = 82.9 pc.

7. Discussion and conclusion

New photoelectric U,B,V and R LCs of RT And obtained from 1997 to 1999 are presented. They were included in a comprehensive study and reanalysis of most of the available observational material.

The true behaviour and causes of the orbital period changes were not solved definitely. There are still three possible explanations of the observed period changes: period jumps caused by instantaneous mass bursts from the primary to the secondary component, continuous period decrease due to mass transfer or magnetic braking combined with the LITE caused by a possible third body or the LITE caused by the third and fourth body in the system. Although the first explanation is most suitable for the future forecast of the minima, the other possibilities cannot be ruled out.

The radial velocity data compiled from the literature show both real variations caused by the maculation present on both components and discrepancies caused by the different CCF techniques employed. The existence of a small eccentricity found by previous authors from the LCs analysis is not confirmed from the study of RVs.

Simultaneous solution of the RV curves and UBVRIJK LCs without maculation provided two sets of photometric and spectroscopic parameters of the system differing mainly in the inclination and ratio of radii of the components. The χ^2 as well as an additionally performed observational test support the high inclination solution (i = 87.6°$\pm$ 0.1°). In both cases the mean observed U LC shows an additional light during the secondary minimum. There is only a negligible third light present in LCs.

Adopting the high-inclination solution we get the masses of the components as follows: m_1 = 1.10$\pm$ 0.02 $M_\odot$, m_2 = 0.83$\pm$ 0.02 $M_\odot$ and the mass ratio q = 0.752$\pm$0.016. The distance to the system corresponding to the high-inclination solution and zero interstellar absorption is d = 83$\pm$2 pc, close to the Hipparcos value d = 75$\pm$6 pc.

The star-spot analysis of all published LCs suggests a more-or-less random position of starspots on the surface of the primary component, so the idea of two active longitude belts proposed by Zeilik et al. (1989a) is not confirmed. The spot around 270° seems to oscillate about the quadrature position with a period of 6.8 years. The positions of the spots either on the primary or the secondary component is not unique. Two LCs were optimized introducing a starspot on the secondary component. The face-to-face position of the spots on the surface of both components in 1971 indicates the possibility of a mass transfer from the primary to the secondary component through a magnetic bridge connecting both active regions.

Acknowledgements. This work was accomplished during the stay of D.C. and T.P. in Napoli. They would like to thank to OAC and University for support and Prof. P.A. Heckert for providing his original observations. This work has been supported by VEGA Grant 5038/2000.

References

Albayrak B., Özeren F.F., Ekmençi F., 1996, Inf. Bull. Var. Stars No. 4399

Albayrak B., Özeren F.F., Ekmençi F., et al., 1999, Rev. Mex. Astron. Astrofis. 35, 3

Al-Naimiy H.M., 1978, Ap&SS 53, 181
Agerer F., Hübscher J., 1999, Inf. Bull. Var. Stars No. 4711
Ahnert P., 1973, Inf. Bull. Var. Stars No. 786
Arévalo M.J., Lázaro C., Claret A., 1995, AJ 110, 1376
Arévalo M.J., Lázaro C., 1999, AJ 118, 1015
Ashbrook J., 1952, AJ 57, 63
Azarnova T.A., 1955, Astron. Circ. 163, 15
Bakos G.A., Tremko J., 1981, In: Chiosi C., Stalio R. (eds.) Effects of Mass Loss on Stellar Evolution. D. Reidel, Dordrecht, p. 491
Baldinelli L., Benefenati F., Cortelli P., 1973, Inf. Bull. Var. Stars No. 838
Baldinelli L., Ghedini S., 1976, Inf. Bull. Var. Stars No. 1143
Banks T., 1991, Publ. Astron. Soc. Australia 9, 148
Borkovits T., Hegedüs T., 1996, A&AS 120, 63
Borkovits T., Bíró I.B., 1998, Inf. Bull. Var. Stars No. 4633
Bradstreet D.H., 1993, Binary Maker 2.0, Dept. Phys. Sci., Eastern College, St. Davids, PA, USA
Budding E., Zeilik M., 1987, ApJ 319, 827
Budding E., Kadouri T.H., Giménez A., 1982, Ap&SS 88, 453
Caton D.B., Burns W.C., Hawkins R.L., 1991, Inf. Bull. Var. Stars No. 3552
Chochol D., Pribulla T., Teodorani M., et al., 1998, A&A 340, 415
Dapergolas A., Kontizas E., Kontizas M., 1988, Inf. Bull. Var. Stars No. 3267
Dapergolas A., Kontizas E., Kontizas M., 1991, Inf. Bull. Var. Stars No. 3661
Dapergolas A., Kontizas E., Kontizas M., 1992, Inf. Bull. Var. Stars No. 3818
Dapergolas A., Kontizas A., Kontizas M., 1994, Inf. Bull. Var. Stars No. 4036
Deichmueller F., 1901, Astron. Nachr. 157, 31
Dean C.A., 1974, PASP 86, 912
Dempsey R.C., Linsky J.L., Fleming T.A., et al., 1993, ApJS 86, 599
Drake S.A., Simon T., Linsky J.L., 1986, AJ 91, 1229
Dumitrescu A., 1973a, Studii si Cercetari de Astr. 18, 47
Dumitrescu A., 1973b, Inf. Bull. Var. Stars No. 830
Dumitrescu A., 1974, Studii si Cercetari de Astr. 19, 89
Ebersberger J., Pohl E., Kizilirmak A., 1978, Inf. Bull. Var. Stars No. 1449
Eker Z., 1999, ApJ 512, 386
Ghedini S., 1982, Software for Photometric Astronomy. Willmann-Bell Publ. Comp., Richmond
Gordon K., 1948, AJ 53, 198
Gordon K., 1955, AJ 60, 422
Gordon S., Hall S., Ledlow M., et al., 1990, Inf. Bull. Var. Stars No. 3469
Gunn A.G., Hall J.C., Lockwood G.W., et al., 1996, A&A 305, 146
Hall D.S., Kreiner J.M., Shore S.N., 1980, In: Plavec M.J., et al. (eds.) Close Binary Stars: Observations and Interpretations. IAU Symp. 88, D. Reidel, Dordrecht, p. 383
Hanžl D., 1990, Inf. Bull. Var. Stars No. 3423
Hanžl D., 1994, Inf. Bull. Var. Stars No. 4097
Heckert P.A., 1995, Inf. Bull. Var. Stars No. 4224
Heckert P.A., 1996, Inf. Bull. Var. Stars No. 4384
Heckert P.A., 1998, Inf. Bull. Var. Stars No. 4656
Heckert P.A., 1999, private communication
Huisong, T., Xuefu L., 1987, A&A 172, 74
Jordan F., 1929, Publ. Allegheny Obs. 7(2), 160
Johnson H.L., 1966, ARA&A 4, 193
Keskin V., Pohl E., 1989, Inf. Bull. Var. Stars No. 3355
Kizilirmak A., Pohl E., 1969, Astron. Nachr. 291, 111
Kizilirmak A., Pohl E., 1974, Inf. Bull. Var. Stars No. 937
Komžík R., 1999, private communication
Kristenson H., 1967, Bull. Astron. Inst. Czechosl. 18, 261
Kron G.E., 1950, PASP 62, 141
Kukarkin B.V., Kholopov P.N., Artiukhina N.M., et al., 1982, New Catalog of Suspected Variable Stars. Nauka, Moscow
Kwee K.K., van Woerden H., 1956, Bull. Astron. Inst. Nether. 12, 327
Lang K.R., 1992, Astrophysical Data: Planets and Stars. Springer, New York, 138
Latrob M., 1950, Astron. Circ. 100, 17
Lenouvel M., 1951, Publ. Obs. Haute-Provance 2, 1
Lenouvel M., 1957, J. des Obs. 40, 41
Lucy L.B., 1967, Z. f. Astrophys. 65, 89
Lynds B., 1962, ApJS 7, 1
Mancuso S., Milano L., Russo G., et al., 1978, Inf. Bull. Var. Stars No. 1409
Mancuso S., Milano L., Russo G., 1979a, A&AS 36, 415
Mancuso S., Milano L., Russo G., et al., 1979b, A&AS 38, 187
Mancuso S., Milano L., Russo G., et al., 1979c, Ap&SS 66, 475
Milano L., 1981, In: Carling E.B., Kopal Z. (eds.) Photometric and Spectroscopic Binary Systems. D. Reidel, p. 331
Milano L., Russo G., Mancuso S., 1981, A&A 103, 57
Milano L., Mancuso S., Vittone A., et al., 1986, Ap&SS 124, 83
Murnikova V.P., Lemeshchenko N.D., 1981, Perem. Zvezdy 21, 593
Müyesseroğlu Z., Gürol B., Selam S.O., 1996, Inf. Bull. Var. Stars No. 4380
Nijland A., 1931, Bull. Astron. Inst. Nether. 6, 113
Obůrka O., 1964, Bull. Astron. Inst. Czechosl. 15, 250
Obůrka O., 1965, Bull. Astron. Inst. Czechosl. 16, 212
Payne-Gaposchkin C., 1946, ApJ 103, 291
Patkos L., 1980, Inf. Bull. Var. Stars No. 1751
Pohl E., Kizilirmak A., 1964, Astron. Nachr. 288, 69
Pohl E., Kizilirmak A., 1966, Astron. Nachr. 289, 191
Pohl E., Kizilirmak A., 1970, Inf. Bull. Var. Stars No. 456
Pohl E., Kizilirmak A., 1972, Inf. Bull. Var. Stars No. 647
Pohl E., Kizilirmak A., 1976, Inf. Bull. Var. Stars No. 1163
Pohl E., Gulmen C., 1981, Inf. Bull. Var. Stars No. 1924
Pohl E., Evren S., Tümer O., et al., 1982, Inf. Bull. Var. Stars No. 2189
Pohl E., Tunca Z., Gulmen O., et al., 1985, Inf. Bull. Var. Stars No. 2793
Pohl E., Akan M.C., Ibanoğlu C., et al., 1987, Inf. Bull. Var. Stars. No. 3078
Popper D.M., 1994, AJ 108, 1091
Popper D.M., 1998, PASP 110, 919
Pribulla T., Chochol D., Parimucha Š., 1999a, Inf. Bull. Var. Stars No. 4751
Pribulla T., Chochol D., Rovithis-Livaniou H., et al., 1999b, A&A 345, 137
Pribulla T., Chochol D., Parimucha Š., 1999c, Contrib. Astron. Obs. Skalnaté Pleso 29, 111
Rovithis-Livaniou H., Rovithis P., Kalimeris A., et al., 1994, Rom. Astron. J. 4, No. 2, 135
Rucinski M.J., 1969, Acta Astron. 19, 245
Schmidt E.G., 1996, PASP 108, 1105
Stellingwerf R.F., 1978, ApJ 224, 953
Sternberk B., 1927, Publ. Inst. Astron. Univ. Charles de Prague, Ser. II, No. 7, 10
Strassmeier K.G., Hall D.S., Fekel F.C., et al., 1993, A&AS 100, 173
van't Veer F., 1973, A&A 26, 357

Wang X., Lu W., 1993, In: Leung J.C., Nha I.S. (eds.) New Frontiers in Binary Star Research. ASP Conference Series 38, p. 280
Williamon R.M., 1974, PASP 86, 924
Wilson R.E., 1979, ApJ 234, 1054
Wilson R.E., 1992, private communication
Wilson R.E., Devinney E.J., 1971, ApJ 166, 605
Wood F.B., Forbes J.E., 1963, AJ 68, 257
Zeilik M., Elston R., Henson G., et al., 1982, Inf. Bull. Var. Stars No. 2090
Zeilik M., Beckert D., De Blasi C., et al., 1988, Inf. Bull. Var. Stars No. 3173
Zeilik M., Cox D.A., De Blasi C., et al., 1989a, ApJ 345, 991
Zinner E., 1915, Astron. Abh. 4, C5